Groundwater Assessment and Aquifer Characterisation in the Musgrave Province, South Australia: Interpretation of SPECTREM Airborne Electromagnetic Data

Ley-Cooper AY, Munday TJ

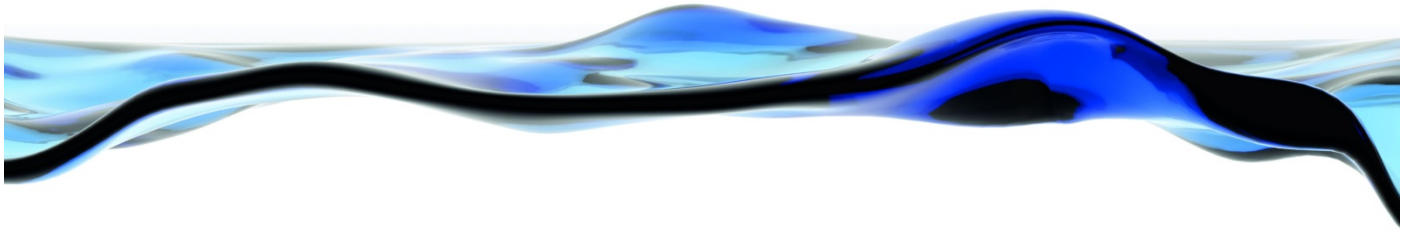

Goyder Institute for Water Research
Technical Report Series No. 13/7

GOYDER INSTITUTE FOR WATER RESEARCH

www.goyderinstitute.org

Goyder Institute for Water Research Technical Report Series ISSN: 1839-2725

The Goyder Institute for Water Research is a partnership between the South Australian Government through the Department for Environment, Water and Natural Resources, CSIRO, Flinders University, the University of Adelaide and the University of South Australia. The Institute will enhance the South Australian Government's capacity to develop and deliver science-based policy solutions in water management. It brings together the best scientists and researchers across Australia to provide expert and independent scientific advice to inform good government water policy and identify future threats and opportunities to water security.

Enquires should be addressed to: Goyder Institute for Water Research
Level 1, Torrens Building
220 Victoria Square, Adelaide, SA, 5000
tel: 08-8303 8952
e-mail: enquiries@goyderinstitute.org

Citation

AY Ley-Cooper and TJ Munday (2013) *Groundwater Assessment and Aquifer Characterization in the Musgrave Province, South Australia: Interpretation of SPECTREM Airborne Electromagnetic Data*, Goyder Institute for Water Research Technical Report Series No. 13/7, Adelaide, South Australia

Copyright

Disclaimer

Executive Summary

This report describes our evaluation of the use of the data from a SPECTREM$_{2000}$ airborne electromagnetic (AEM) survey flown in April 2012 to assess groundwater and aquifers in the Musgrave Province of South Australia. In order to successfully invert the AEM data to conductivity–depth models, and produce maps and profiles we reverse-engineered the process by which Spectrem Air Ltd. subtracts the primary field from measured data. First, we reinstate the removed primary field estimate and convert the data from ppm units to Teslas. Next, we then simultaneously invert the X and Z component data, to solve for a 1D layered conductivity model and receiver position, using Geoscience Australia's inversion algorithm. High-altitude data and synthetic forward models were also analysed to better understand noise levels in the SPECTREM$_{2000}$ data. The final products of this study are a suite of conductivity–depth maps and sections generated from inverted data for two areas in the Musgrave Province. Comparisons of inverted models derived from SPECTREM$_{2000}$ data with those derived from TEMPEST, VTEM and SkyTEM data are also included. An important outcome of this work is the knowledge gained about the capabilities and data quality of the SPECTREM$_{2000}$ system, which is relatively new to Australia.

Acknowledgements

We especially want to thank Ross Brodie from Geoscience Australia, who has been involved in the process of reinstating the primary file into the SPECTREM data and helping prepare it in order to be inverted with the GA-LEI inversion algorithm.

We thank Peter Leggatt, Phil Kilnkert, Braam Duplo, Luis Palome, Jaco Smith and Nirocca Devkurran of Spectrem Air Ltd. for assistance with data processing and helping us sort out data formats, units and other peculiarities that are intrinsic with the handling of AEM data from the SPECTREM system.

We also thank Musgrave Minerals for provision of TEMPEST and VTEM data and their insights into AEM data from the Musgrave Province.

Special appreciation goes to Tania Abdat and Travis Naughton from CSIRO, for the GIS and graphics services they provided to help complete this report.

Table of contents

List of Figures

Tables

Introduction

Background

Part of the Goyder Institute's (www.goyderinstitute.org) Facilitating Long-term Outback Water Solutions (G-FLOWS) project concerns the use of regional (State and Federal agency) and local-scale (exploration company) geophysical data sets to help develop a hydrogeological framework for the South Australia's arid regions, where there is often a paucity of data on groundwater and surface water.

In the Musgrave Province of South Australia (Figure 1), local scale (historical and more recent) airborne electromagnetic (AEM) data sets acquired primarily for minerals exploration have been re-processed and reinterpreted to develop hydrogeological conceptual models in support of a regional scale water resource assessment. Historical data sets include those acquired by the TEMPEST (Lane et al., 2000), HoistEM (Boyd, 2004) and VTEM (Witherly et al., 2004) AEM systems. Co-incident data from several new AEM systems, specifically the SkyTEM^{508} (Sørensen and Auken, 2003) and the SPECTREM$_{2000}$ (Leggatt et al., 2000) have also been acquired to inform options for further pre-competitive AEM data collection, supporting both mineral exploration and groundwater resource assessment in the region.

Objectives

This report documents the development of processing and interpretation procedures that have been defined to handle data from the SPECTREM AEM system. Data from this system has been acquired in the Musgrave Province and procedures described here are relevant to their hydrogeological interpretation.

Spectrem Air Ltd was commissioned to survey two small trial areas in the Musgrave Province in 2012 using their SPECTREM $_{2000}$ airborne electromagnetic (AEM) system. To facilitate evaluation of the SPECTREM$_{2000}$ system, flight paths for the two surveys were deliberately placed to overlap previous TEMPEST,VTEM AEM and SkyTEM surveys.

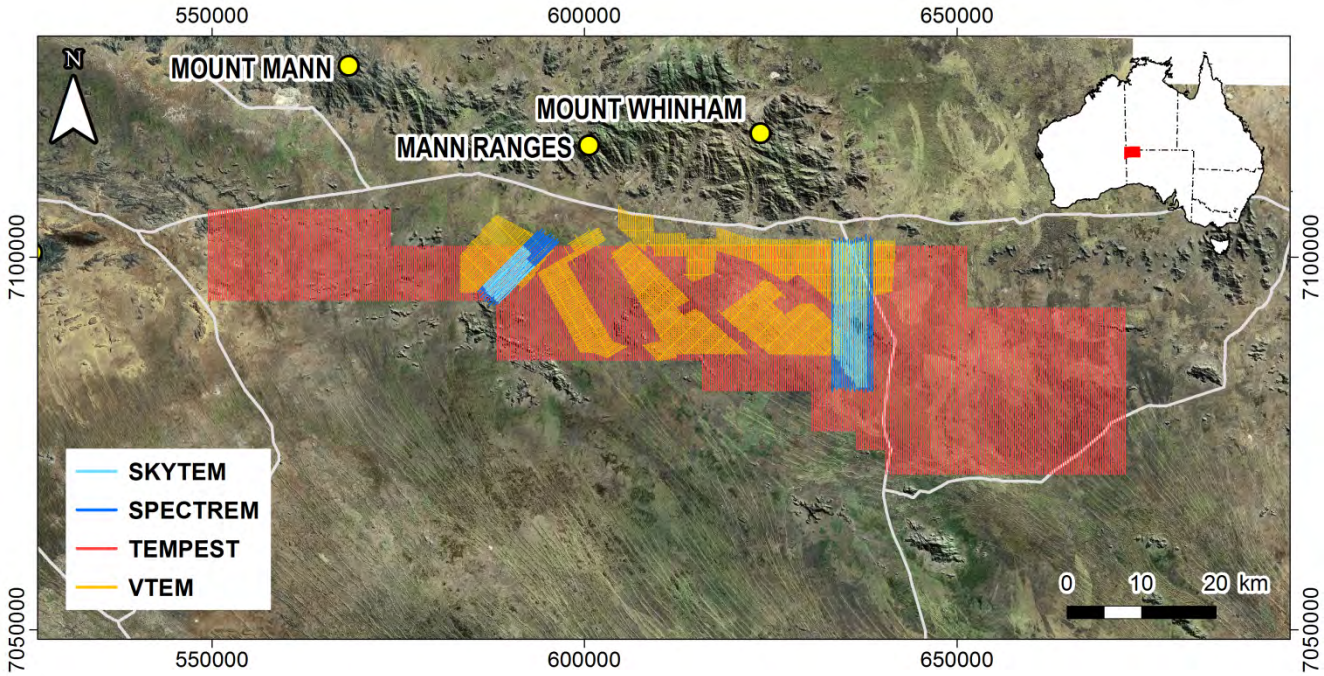

Figure 1. SPECTREM, SkyTEM and historical VTEM and TEMPEST flight paths overlaid on an orthophotograph of the area.

This report represents the outcomes of a collaborative initiative between Geoscience Australia (GA) and CSIRO, developed under the auspices of the G-FLOWS project, with the collaboration aimed at gaining an understanding of the capabilities of the SPECTREM$_{2000}$ system for mapping in Australian conditions. The survey was flown according to a set of mandatory technical specifications outlined in Geoscience Australia's deed of standing offer with contractors who provide AEM technologies for Government surveys. Using production data acquired over Australian ground to assess the performance of the SPECTREM system against technical specifications outlined in the deed is of interest to both CSIRO and GA, as it is a way of ensuring quality control on the acquired data.

Based on our experience, an appropriate way to assess the capabilities of an AEM system is to determine whether our conceptual system characterisation, applied to data recorded under standard survey conditions, can be used to emulate a simple layered-earth geo-electrical model. Such an exercise yields the elements needed for inversion of the survey data. Results from inversion of SPECTREM$_{2000}$ data discussed here are seen as critical in gaining a better understanding on regolith variability, aquifer geometry and groundwater characteristics.

The SPECTREM airborne electromagnetic system

Historical context

The SPECTREM AEM system is a fixed-wing, time domain AEM system that has been used in North America, Africa and Australia since 1989. An early prototype was described by Annan (1986). Since 1989, the system has undergone a series of modifications (Klinkert et al., 1996; Klinkert et al., 1997) to reach its current operational state, as described by Leggatt et al. (2000).

In fixed wing towed-bird systems, the transmitter is a multi-turn loop suspended between the aircraft's nose, wings and tail. The receiver consists of orthogonal coils that are towed in a 'bird' behind the aircraft. The position of the transmitter relative to the receiver defines the system's geometry (Figure 2).

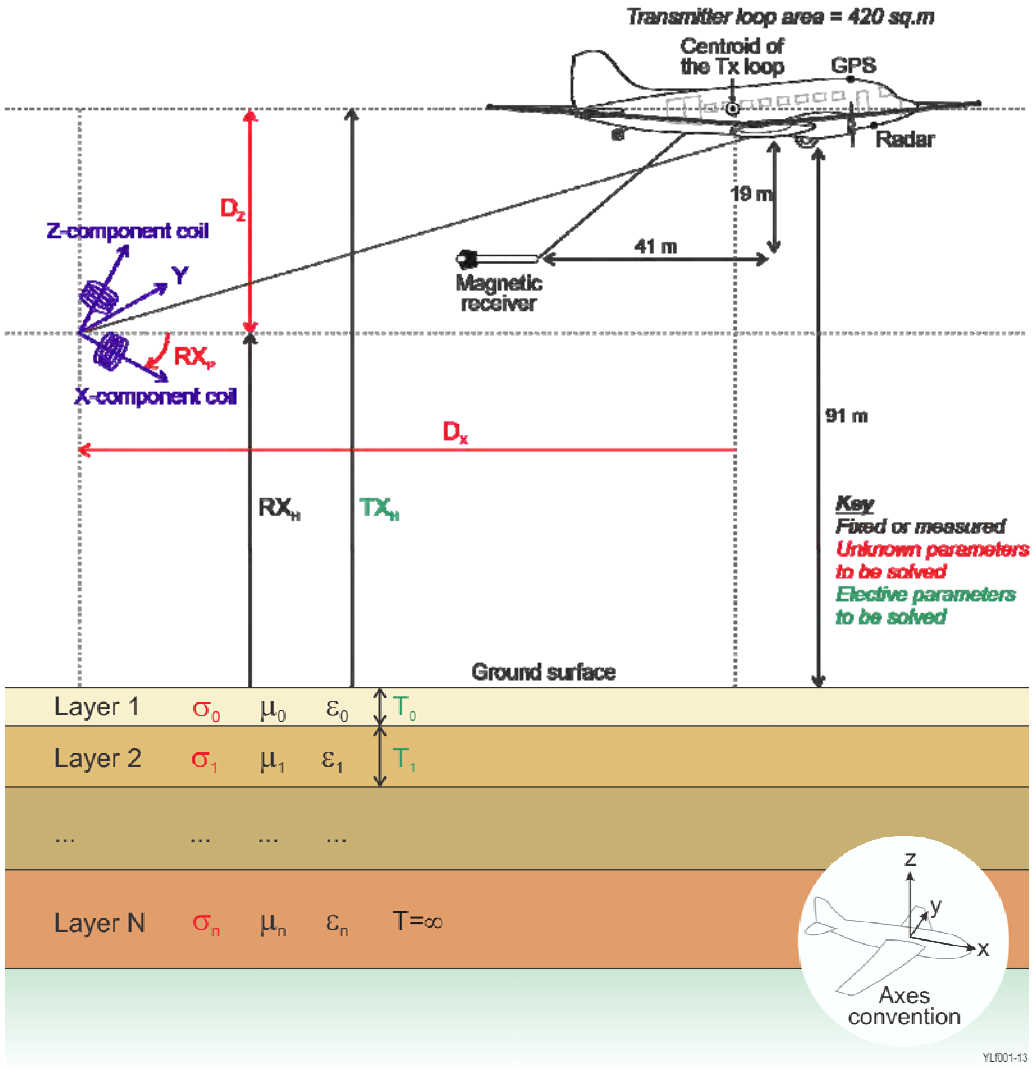

Figure 2: Schematic representation of the system's geometry, sensors positions and the input / output parameters used in the inversion framework for the GA-LEI inversion of SPECTREM$_{2000}$ data. The conventions for rotation axes are also described (inset figure lower right). Red elements are the unknowns to be solved, including conductivity (σ), receiver pitch (RXp), transmitter–receiver horizontal (Dz) and vertical (Dx) separation. Layer thickness (Tn) and transmitter height (TX_H) have been marked in green as elective parameters to be solved. All fixed measurements are shown in black.

The SPECTREM$_{2000}$ system has reportedly been used successfully to map and discriminate targeted geological units to depths of hundreds of metres in the presence of conductive cover (Leggatt et al., 2000; Pare et al., 2012). The system has been specifically designed to map both high-conductance bodies and near-surface conductors. Resolution is dependent on the nature of the regolith cover, the specific lateral and vertical extent of target bodies and their own particular electrical properties.

System description

The SPECTREM$_{2000}$ system simultaneously measures electromagnetic, gamma-ray spectrometric and total field magnetic data; both the electromagnetic and magnetic sensors are towed behind the aircraft. In this report, we discuss only the EM data. The system geometry and other specifications are provided in Table 1. The sensors' position and relative geometry are shown in Figure 2.

From here on we will refer to the SPECTREM$_{2000}$ system just as SPECTREM and Spectrem Air to the company Spectrem Air Ltd. who developed the system and who are responsible for data collection, its quality, processing and delivery.

Electromagnetic sensors

The SPECTREM system employs a bipolar, full duty-cycle, and an approximately square-wave current pulse, with selectable base frequencies of 25 Hz and higher. The transmitter current and the voltages in the X- and Z-component receiver coils are continuously recorded (streamed) at 76.8 kHz. Through a sequence of data processing steps (Leggatt et al., 2000) each 0.2s (representing a sample on the ground approximately every 15 m) stack of streamed voltage data, which contain both primary and secondary contributions, are transformed into soundings or decays representing the estimated secondary magnetic B-field. Each sounding contains 10 windows (gates) with centre times ranging from 0.026 to 16.654 ms. The processed secondary field data are presented in units of parts per million (ppm) of the corresponding X- or Z-component of the high altitude reference primary magnetic field.

Theoretical modelling and analysis by Liu (1998), who assessed the advantages of using a square waveform, and Smith (1998), who examined the merits of an AEM system's ability to measure during the on-time, were considered during the design of SPECTREM$_{2000}$. The system has a high power transmitter and records data continuously, elements that make it an interesting candidate for mineral and groundwater exploration and for environmental assessments.

Table 1 SPECTREM system specifications for the Musgrave survey

EM system				
Transmitter height above ground	91 m			
Tx–Rx vertical separation	41 m (nominal value)			
Tx–Rx horizontal separation	121 m (nominal value)			
Transmitter coil axis	Vertical			
Receiver coil axes	X – horizontal, parallel to flight direction; Z – vertical Y : horizontal, perpendicular to flight direction Z : vertical			
Current waveform	Square wave			
Base frequency	25 Hz			
Transmitter loop area	420 m^2			
RMS current	960 A			
RMS dipole moment	400 000 $A.m^2$			
Digitising rate @ 25 Hz	38 400 Hz per component			
Recording rate	5 Hz (output rate of stacking filter)			
Number of windows	9 per component (plus primary field estimate, discussed later)			
Window distribution	Pseudo-binary			
Window times (25 Hz)				
Window number	Start (ms)	End (ms)	Centre (ms)	Width (ms)
1	0.0130	0.0391	0.0260	0.0261
2	0.0521	0.0781	0.0651	0.0260
3	0.1042	0.1823	0.14325	0.0781
4	0.2083	0.3906	0.29945	0.1823
5	0.4167	0.8073	0.6120	0.3906
6	0.8333	1.6406	1.23695	0.8073
7	1.6667	3.3073	2.4870	1.6406
8	3.3333	6.6406	4.98695	3.3073
9	6.6667	13.3073	9.9870	6.6406
10 (Primary field)	13.3333	19.9740	16.6536	6.6667
Magnetic system				
Bird height above ground	72 m			
Bird location	19 m below and 41 m behind centre of aircraft			
Sensor	Scintrex CS-2 Sensor with Spectrem Counter/Sync System			
Recording Rate	5 Hz			
Sensitivity / Resolution	0.01 nT / 0.1 nT			
Positioning system on aircraft				
Sensor	Novatel RT-20 GPS receiver with Fugro Omnistar differential corrections			
Recording Rate	5 Hz			
Other sensors				
Radar altitude	Collins, 5 Hz sampling at 0.3 m resolution			
Laser altitude	Riegl, 5 Hz sampling at 0.03 m resolution			
Barometric pressure	Rose Mount, 1 Hz sampling			
Temperature (outside air) temp)	PT-100 RTD, 1 Hz sampling			
Analogue chart recorder	RMS GR-33			

Transmitter position and geometry

Pitch, roll and yaw are three angles that define the orientation of the transmitter loop moment vector (only pitch and roll are measured). The pitch and roll are the angles measured between the transmitter loop and the horizon (Figure 2), the pitch angle is defined as a measure of rotation about the x-axis, and the roll angle is the rotation about the y-axis. Both pitch and roll are zero when the z-axis is vertical. The convention adopted by Spectrem Air is that aircraft nose up indicates a positive pitch angle, and aircraft left wing up indicates a positive roll angle. By taking tilt measurements on the ground Spectrem Air have established that the airplane tilt angle meters give correct angles for the transmitter (Tx) -loop, to within 0.01°. We assumed that radar altimeters can measure with accuracy of up to 1 m. Therefore, when inverting SPECTREM data we have assumed transmitter (Tx) geometry is well defined and allowed the inversion to solve only for vertical and horizontal Tx–Rx separation and for receiver coil pitch.

The laser altimeter (ranger finder) on the aircraft measures slant range rather than altitude. The reported laser altimeter values are corrected for aircraft pitch and roll as follows:

$$\text{las\_alt} = (\text{slant range}) * \cos(\text{pitch}) * \cos(\text{roll}). \quad (1)$$

The transmitter loop centroid is 1.4 m above the radar altimeter antenna. Both the radar altimeter antenna and the laser altimeter lens are at approximately the same level inside the aircraft, below the transmitter loop centroid. The transmitter loop terrain clearance is the height of the Tx loop centroid above the ground, that is:

$$\text{Tx clearance} = \text{rad}_{\text{alt}} + 1.4 \text{ m}. \quad (2)$$

The GPS antenna is 2.49 m above the radar altimeter antenna, so ground elevation (above the geoid) was calculated as:

$$\text{Ground elevation} = \text{GPS\_alt} - \text{rad\_alt} - 2.49. \quad (3)$$

Data assessment and further analysis

System geometry and its implications

For SPECTREM$_{2000}$ data, the system transfer function is derived by recording the transmitted current and received waveform at high altitude in the absence of a ground response. The transmitter loop waveform is known because the current waveform is monitored and the transmitter loop area is known. However, the primary field cannot be precisely predicted at each sounding because elements of the Transmitter–Receiver (Tx-Rx) geometry are not measured.

A frequently experienced issue with AEM systems (Smiarowski et al., 2010; Smith, 2001a) is that the total response measured in the receiver coils (Rx) can never be perfectly decomposed into "its primary response, due to direct induction from the transmitter loop Tx, and the secondary response, due to eddy currents induced in the ground.".

For an AEM system that records only in the off-time, when there is theoretically no primary-field, the system geometry still needs to be known for proper quantitative interpretation of the secondary ground response. If the relative offsets and orientations of the Tx and Rx (i.e., the system geometry) could be measured dynamically in flight with sufficient accuracy, the primary field contribution could be calculated analytically and subtracted from the total response to yield an accurate secondary response.

The geometry problem is partially alleviated for the helicopter EM systems that tow the Tx and Rx in the same flexible (e.g., VTEM, HoistEM) or relatively rigid (e.g., SkyTEM, AEROTEM and RESOLVE) assemblies. For these systems, the rigidity of the frame will determine how representative the on-ground measured geometry is of the in-flight geometry. The use of null-coupled Tx and Rx (e.g., SkyTEM) and bucking coils (e.g., RESOLVE, AEROTEM and VTEM) reduce the influence of the primary field. Nevertheless, because of the proximity of the Rx to the Tx, even minute variations in the geometry during flight, for example as a result from turbulence, can substantially reduce the effectiveness of null-coupling and bucking.

Imprecise knowledge of the Tx-Rx offsets and orientation of the Rx bird is a particular problem for fixed-wing towed receiver (bird) systems (e.g., TEMPEST, GEOTEM, SPECTREM) whose geometry varies continuously throughout flight. For these systems, the Tx height above ground and orientation (roll, pitch and yaw) can typically be measured. However, despite efforts to monitor the bird offset and orientation in fixed-wing systems (e.g. Smith,2001a), this has not so far been achieved with sufficient precision to allow accurate primary field removal.

Schemes used for estimating the primary and secondary contributions in GEOTEM (Smith, 2001b), TEMPEST (Lane et al., 2000) and SPECTREM (Leggatt et al., 2000) data processing all make assumptions about subsurface conductivity. When estimated secondary field data from such processing schemes are used in quantitative conductivity depth imaging (CDI) or layered earth inversion (LEI) algorithms, it is routinely found that the X- and Z-component data cannot be fitted simultaneously with a realistic conductivity model consistent with prior information. In some cases, it is not possible to fit any conductivity model to the data. Sometimes the X- and Z-component data can be fitted independently, but to different conductivity-depth models. The problem usually stems from an inaccurate decomposition of the primary and secondary field in the initial data processing, and the subsequent incorrect estimate of the system geometry calculated from an inaccurate primary field.

Various inversion algorithms have been developed to deal with this problem. They address the issue by solving for unknown elements of the fixed-wing AEM system geometry (or primary field) and propose a conductivity model (e.g., Satell, 2004; Lane et al., 2004).

Synthetic Modelling

Accurate knowledge of the position and orientation of the receiver bird is important for primary-field removal and also for precision in the modelling of field responses. As the bird position fluctuates, so too will the primary and secondary fields measured at the receiver. The (Tx–Rx) coil separation for each sounding can vary considerably and are dependent on flight conditions. Of particular significance is that if these offsets are not accurately known, either by measurement or calculation from field responses, they can have a considerable influence on the modelling of the near surface conditions.

To illustrate the effects of geometry variations, we computed a suite of forward responses over two conductivity models for a range of Tx-Rx offsets (Figure 3). Model a) shows responses from one of the computed models, assuming a 5 m thick (300 ms/m) cover over a 50 m thick (500 mS/m) layer below it, followed by a resistive basement. It is noted that the resulting ground responses varies primarily in the in the early time channels. These results suggest that a given geological structure could actually be characterised by a range of alternative models, by failing to take account of the relative positions of the transmitter and receiver.

We see similar effects in the early-time parts of the decays, when changing the conductive properties in this simplified three layer modelling representation of the regolith cover (Figure 3 model b). For all the forward-model calculations from the different models we used high-altitude estimated system noise levels, which will discussed further in this report, and fixed all other parameters including Rx orientations.

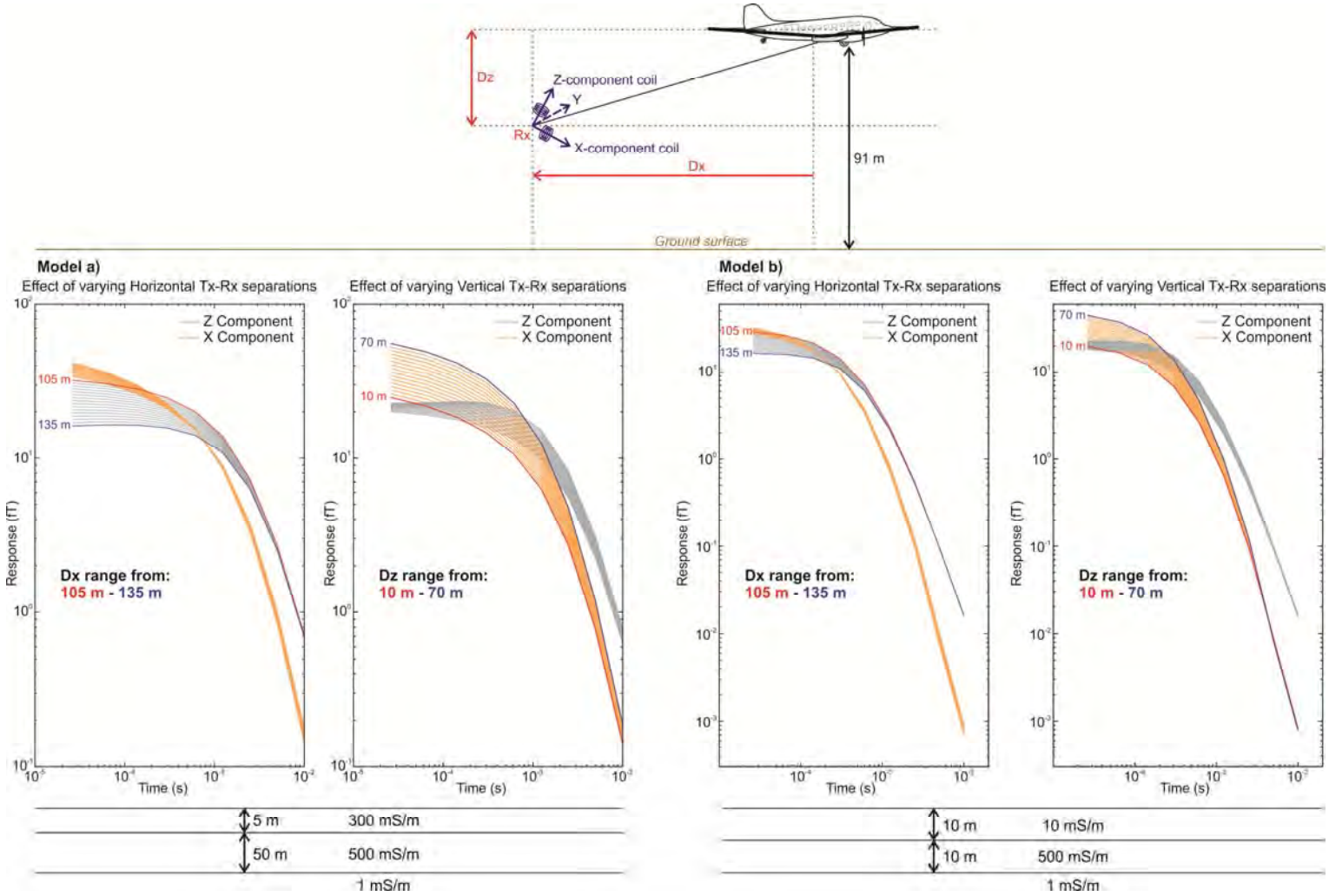

Figure 3. Responses from a synthetic three-layer model, calculated by varying the D_x (horizontal) distance between the receiver bird and the transmitter between 105 to 135 m (left panels models a and b), and the vertical (D_z) separation in 2 m increments from 10 to 70 m (right panels models a and b). Early time responses are those most affected, showing the greatest variability, thereby hindering the system's ability to resolve near-surface, regolith related features. Models a) and b) are synthetic representations of the regolith cover. Responses are calculated by varying the relative distances between the receiver bird and the transmitter

Standard data processing by Spectrem Air reports nominal values of transmitter-receiver vertical and horizontal separations calculated from mean values during high-altitude lines flown at the beginning and end of each survey day. For the Musgrave Province survey data, separations computed from airspeed were also provided. Appendix II in this report explains how we estimated the sensors' relative positions calculated by inversion and from measured transmitter pitch and roll at every sample using parameters derived from the calculated high-altitude primary field data.

Knowledge of the system's Tx-Rx separations can be gained by at least three methods. When using airspeed in the calculations, individual values for each fiducial are estimated from a camera mounted on the aircraft. Last-window estimates values can be reconstructed from primary-field calculations. Finally, values can be determined by inversion, setting the separation as a free parameter in the inversion algorithm. A comparison nominal separations and values derived by (a) airspeed variation, (b) last window, and (c) as an unknown parameter in a layered-earth inversion are show in Figure 4.

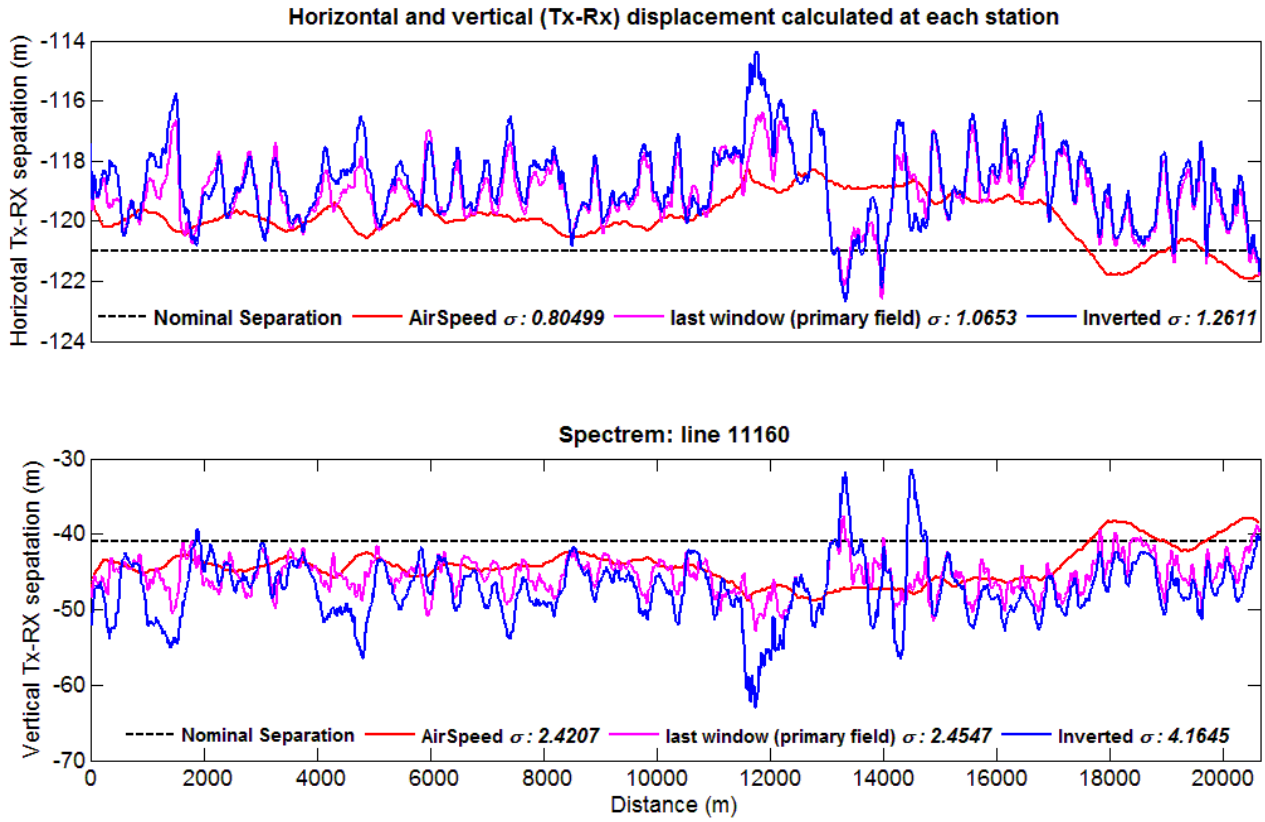

Figure 4. Horizontal (top panel) and vertical (lower panel) transmitter–receiver (Tx–Rx) separations estimated at each fiducial over a 20 km line. Separations and their respective standard deviations were calculated by airspeed (red), last window (magenta), inversion (blue) against the nominal separation (black dashed line).

Transmitter–receiver separations calculated from airspeed using the aircraft mounted camera appear to be lower frequency and have the lowest σ (standard deviation) from all the estimations, which implies camera-based separations are more stable than the other two methods. Unfortunately, camera mounted estimations are not routinely calculated.

To demonstrate the effects of geometry, on the left hand panel of Figure 5, we show X- (grey) and Z-component (black) SPECTREM data with error bars. The data were inverted to 30-layer models using system configurations. In the first configuration, the system geometry was fixed at the high altitude reference geometry. The best fitting conductivity model and its forward response are shown, in blue, on the right and left panels respectively. In the second system configuration, the system geometry was treated as a parameter to be inverted and the best fitting model and its response are now shown in red. The better fitting model results from the inversion where the system geometry was allowed to vary, emphasising the point that making use of the reference, or nominal geometry may yield results that are not be consistent with the data.

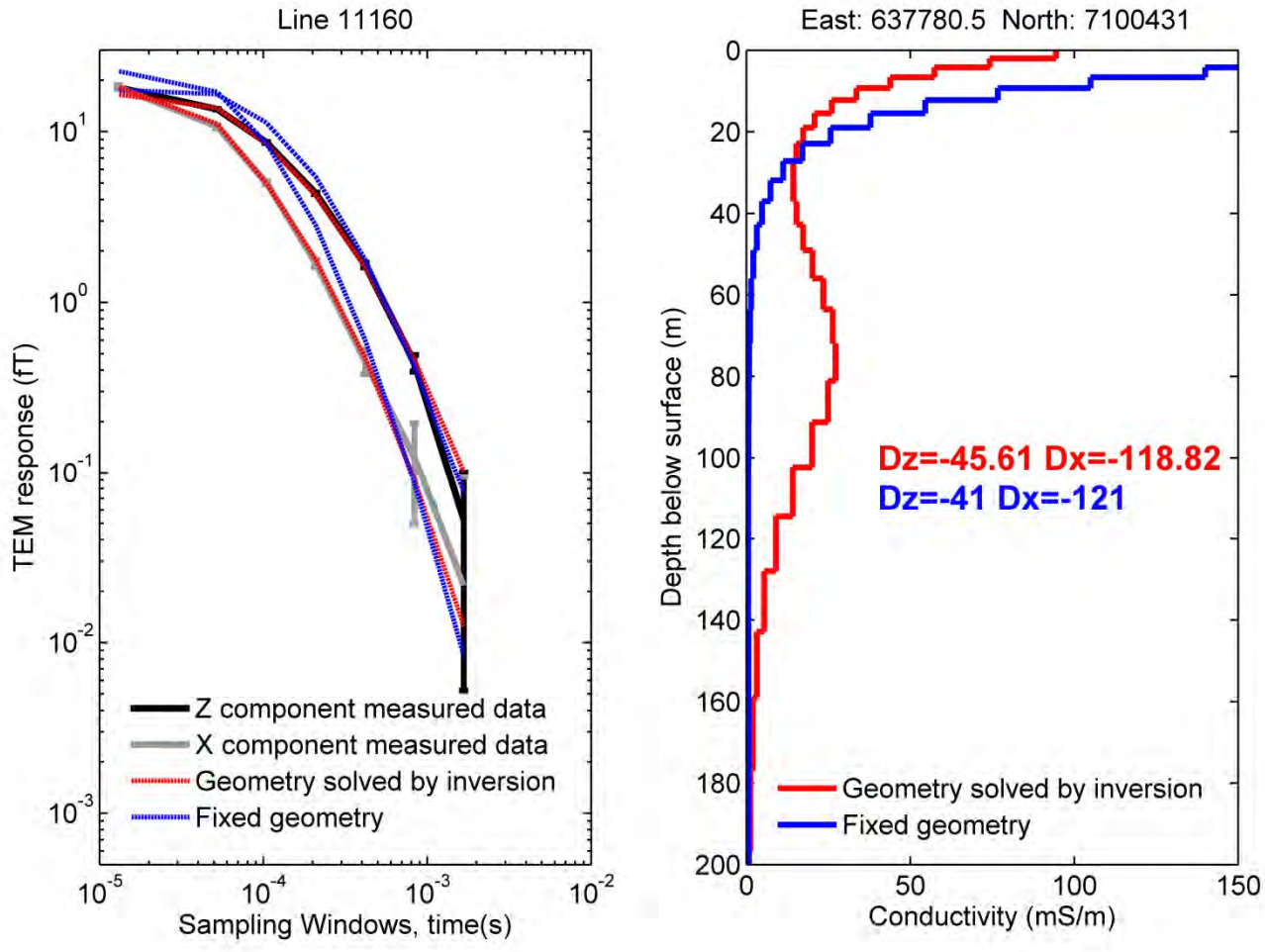

Figure 5. Inversion results for one sounding on line 11160. The grey and black decays on the left hand panel are X and Z component total field data plotted with each time gate's associated error-bar. Also shown are responses of the best fitting 30 layer forward models resulting from inversions where the geometry remained fixed (blue), and was included to be solved for in the inversion (red). The right hand panel shows the corresponding best fit conductivity-depth models in the same colours.

Noise estimates

High-altitude flights were made at the beginning and end of each day of production in order to estimate calibration and primary-field data. It is assumed that at high altitudes the ground response is close to zero. However, this is rarely the case in weathered environments such as Australia where the regolith is often characterised by a strong conductive EM response. To better understand the effects of conductive near surface layers, we modelled the responses expected for the modelled SPECTREM system when flying at an altitude of 1000 m (Figure 6 panel a) and at a normal survey altitude of 90 m (Figure 6 panel b). Model a) has a 10 m thick conductive layer at surface. Model b) has the same conductive layer at a 1000 m depth.

The blue bands in the left panels of Figure 6 show the maximum permissible threshold noise levels for Z component (the noise floor). These noise levels were established from daily high-altitude flights during the survey in the Musgrave. Absolute values for each channels noise levels are shown in Figure A1 of Appendix II and were estimated using a multiplicative and additive component as suggested in Green and Lane (2003). In Figure 6 the conductivity model a) shows that Z-component values are above the calculated noise levels, at least for the first five windows. According to our forward modelling calculations the SPECTREM system should detect a 1000 mS/m, 10-m-thick regolith layer located at the surface when flying at an altitude of 1000 m. The system's sensitivity has implications on primary-field removal procedures and on assumptions made on noise level estimations. The forward model results suggest that altitude-based primary field removal methods are prone to error in high conductivity regions, particularly if flights are flown over weathered terrains. Such regions are common over most areas of Australia.

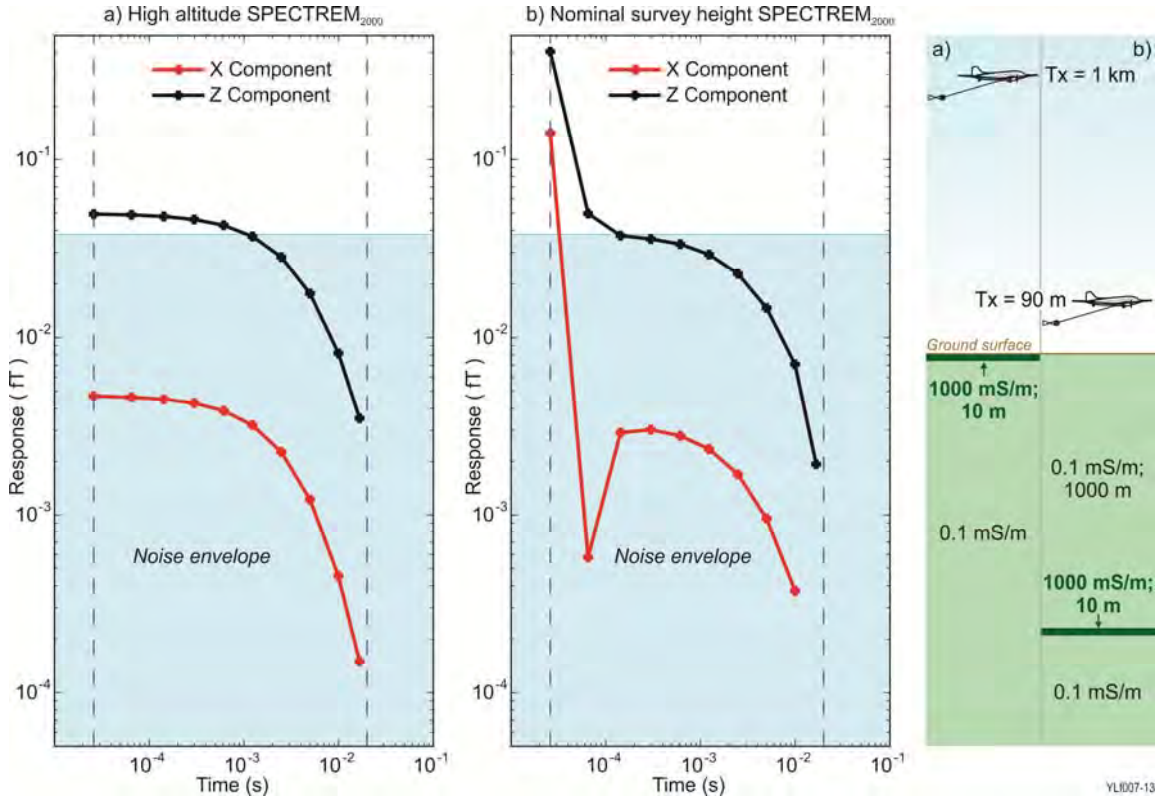

Figure 6. Modelled X and Z component responses, in panel a) from a transmitter dipole at 1000 m altitude over a 10-m-thick of 1000 mS/m conductivity conductor at the surface. Panel b) shows responses from dipole at a nominal altitude of 90; with the same 1000 mS/m conductor at a depth of 1000 m below a resistive (1 mS/m) host.

Another procedure commonly followed when assessing a surveys' noise levels, is to determine patches of "resistive" ground. Then relative noise levels are estimated, assuming currents have migrated far enough and no response from deep conductors will have major influence on the windowed channels. Our second model panel b) in Figure 6 shows the same conductive layer now buried at a depth of 1000 m in a very resistive (0.1 mS/m) host. The layer still might influence the response of the Z-component, of a system flown at a 90 m survey height. This implies that a response which has travelled over, what we assume might be a thick resistive segment of ground cannot always be regarded to be uninfluenced by deep conductive sources.

Inversions and fast transforms

Assessment of AEM data is commonly carried out qualitatively on soundings which are plotted as a continuous profile of channels. Anomalous amplitudes and shapes are then visually compared to the responses from simple bodies such as thin sheets, plates, spheres and other geometric bodies. Further analysis can be done by parametric modelling which allows calculation of strikes, dips and other geometric dimensions. A rguably, the use of AEM data exclusively for isolated anomaly modelling undervalues the method's full potential (Worrall et al., 1998). The high spatial density and large area coverage of AEM data enables regional geological mapping, particularly if there is sufficient contrast in the responses of subsurface formations. AEM responses can be converted to estimates of subsurface conductivity and depth by inversion which permits a quantitative assessment of the changes in the geo-electrical properties of the subsurface materials.

We consider that an important part of interpreting AEM data is to understand how the data were acquired, sampled, filtered and processed. When all data acquisition and processing parameters are considered and quantified (Christiansen et al., 2011; Davis and Macnae, 2008; Smith and Neil, 2012), then ground response can be accurately modelled and subsequently inverted.

In this report, the processing and inversion of the Musgrave Province AEM data, and the sections and maps generated for various depths below the ground surface, are based on three algorithms that transform AEM data to layered models of conductivity and depth. These include:

- 1D-layered earth (1D LEI) sample-by-sample (SBS) inversion models (Lane et al., 2004),
- Conductivity-Depth transforms by developed and applied by Spectrem Air (Leggatt and Pendock, 1993),
- Conductivity–depth images (CDIs) derived using the EMFlow algorithm (Macnae et al., 1998).

Layered-earth models allow comparatively rapid forward modelling and inversion in comparison to the more general 2D or 3D earth models, which commonly require numerical solutions. Layered-earth models provide reliable approximations of the real earth in stratified geological environments where the scale of lateral variation is greater than the footprint of the AEM system (Reid and Vrbancich, 2004). A further argument for the use of a 1D model is that electromagnetic data are inherently ambiguous. The real earth conductivity distribution is very complex. Inverting for 2D and 3D conductivity distributions introduces a large number of unknowns.

There are several advantages of individually inverting each sounding with a 1D algorithm. Data misfit on a sample-by-sample basis encourages revisiting the data at specific locations, which in-turn allows assessment of data quality. In remote parts of Australia, large data misfits and inversion artefacts are seldom the products of anthropogenic noise; and they mostly represent rapid lithological change, dipping layers, or other effects of lateral conductivity contrast. Imposing lateral inversion constraints to ensure layer continuity (Viezzoli et al., 2008) or sub-sampling the AEM data because of redundancy (Cox et al., 2010) can mask sharp boundaries and compromise the inversion results by enforcing lateral consistency. This can be a disadvantage, particularly for mineral exploration. Nevertheless, lateral constraints are routinely used around the world and can work well specially when employed for groundwater and aquifer mapping (Auken and Christiansen, 2004).

Geoscience Australia's layered-earth inversion algorithm (GA-LEI)

To gain an understanding of data acquired by the SPECTREM AEM system, we used Geoscience Australia's layered-earth sample-by-sample inversion (GA-LEI) as the main inversion algorithm used for comparisons. This algorithm, conceptualised by Lane et al. (2004), was developed by Brodie (2009). It was designed to solve the non-linear problem of obtaining subsurface values of conductivity from a measured AEM response while accounting for geometric unknowns. It is based on an idealised layered-earth model calculation at each sounding, and assumes individual layers are laterally homogenous over an extent as wide, at least as the annulus of resolution of the airborne system, which is a surface radius of approximately 80 m for SPECTREM (Ley-Cooper et al., 2010).

The GA-LEI inversion algorithm is capable of inverting total (primary plus secondary) field data to solve for the Tx-Rx horizontal and vertical offsets as well as the Rx pitch along with a 1D conductivity model. In doing so, it circumvents the potential pitfalls, summarized earlier (see Section on Data Assessment) of estimating the primary field and quantitative interpretation in two sequential steps. Therefore we first need to reinstate the primary-field, back into our dataset, that was removed during the original data processing.

In the original processing of the SPECTREM dataset, the kth window of the X-component sounding $\mathrm{X}_{\mathrm{k}}^{\mathrm{ppm}}$ is given as an estimated secondary field in units of parts per million (ppm) of the unipolar (i.e., zero-to-peak) primary-field measured on the high altitude reference line X_{ref}. It is calculated as

$$\mathrm{X}_{\mathrm{k}}^{\mathrm{ppm}} = 1/2\left[\frac{10^6(X_k - X_{10})}{X_{ref}}\right] \quad (4)$$

where X_k is the total survey altitude response in the kth window prior to primary field removal and conversion to ppm. Thus, the primary field estimate X_{10} is the total response in the last (10th) window. Therefore, usually only nine windows of ppm data are delivered since the tenth will always be zero. The division by 2 simply converts the bipolar (peak-to-peak) current step to a unipolar (peak-to-zero) current step response. The removed primary was delivered in the dataset as the so-called coupling channel, given by,

$$\mathrm{X}_{\mathrm{coupled}}^{\mathrm{ppm}} = \frac{10^6(X_{10})}{X_{ref}} \quad (5)$$

which is used to reconstruct the total response.

For the SPECTREM system, there are two unknown amplitude scaling factors that would relate a given transmitter current to resulting X- and Z-component receiver responses. They are dependent on the amplifier gains and other conversions (Braam du Plooy, pers. comm., June 2012). Without these scaling factors, or alternatively exact knowledge of the Tx-Rx offsets, we cannot convert the data from relative ppm units to the required absolute B-field units (e.g., in Teslas). This is somewhat different to the case for the LEI inversion of TEMPEST data. According to Lane (2000), the TEMPEST system has been calibrated such that it allows conversion of the processed data to absolute units of Tesla.

We therefore used the average high altitude reference line Tx-Rx horizontal and vertical offsets, $\mathrm{D_X^{ref}} = 121\ \mathrm{m}$ and $\mathrm{D_z^{ref}} = 41\ \mathrm{m}$, that were estimated by Spectrem Air (using cameras, a laser range finder and knowledge of the tow cable length) to constrain the unknown scaling factors. Using these offset values along with the measured Tx roll and pitch angles and assuming a straight and level Rx bird (i.e., zero roll, pitch and yaw), we calculated the theoretical unit magnetic dipole field at the receiver in units of femto Tesla (fT) for the X and Z-components as $\mathrm{X_{ref}^{fT}}$ and $\mathrm{Z_{ref}^{fT}}$.

Since the ratios of the survey altitude fields to the high altitude reference fields are independent of the units used, that is,

$$\mathrm{X_k^{fT}}\Big/_{\mathrm{X_{ref}^{fT}}} = \mathrm{X_k}\Big/_{\mathrm{X_{ref}}} \tag{6}$$

by combining equations 4,5 and 6 we can reconstruct the total field in units of femtoTeslas as,

$$\mathrm{X_k^{fT}} = (2\mathrm{X_k^{ppm}} + \mathrm{X_{coupled}^{ppm}})\mathrm{X_{ref}^{fT}} \Big/_{10^6} \tag{7}$$

An exactly analogous reconstruction is performed for the Z-component data,

$$\mathrm{Z_k^{fT}} = (2\mathrm{Z_k^{ppm}} + \mathrm{Z_{coupled}^{ppm}})\mathrm{Z_{ref}^{fT}} \Big/_{10^6} \tag{8}$$

Equations 7 and 8 give the reconstructed total magnetic B-field in units of femtoTeslas (fT/Am^2) that were input into the GA-LEI algorithm. In doing this we have had to assume that the estimated high altitude reference line geometry is correct. However, in our GA-LEI inversion, we also solve for new values of the horizontal (D_x) and vertical (D_z) offsets as well as the receiver pitch (RX_p) for every sounding, simultaneously with a 1D conductivity model. Parameters used for the inversion of SPECTREM data are shown in Figure 2.

Spectrem Air Ltd. 1D conductivity transforms

Spectrem Air's in-house conductivity-image software was developed by Leggatt and Pendock (1993), it incorporates a determination measure of one model over another in situations where both can fit the data. The algorithm is based on the assumption that a step transient waveform over a horizontally layered earth induces a current flow in the ground, and the resultant magnetic field can be approximated by the image of the transmitter reflected at surface and receding downwards at constant velocity. Polzer (1985) showed that this model can be expressed as

$$t_k \mu_0 = \int_0^{h_k} (h_k - z)\sigma(z)dz \tag{9}$$

where $h_k$is half the depth below the surface at time t_k after the step transient and $\sigma(z)$ is the conductivity of the layered earth below the surface at depth z. The algorithm discretises the proposed convolution function and solves the undermined linear system yielding many possible solutions that fit the data, and then proposes the solution with maximum entropy as the final model.

Conductivity–depth images derived using the EMFlow algorithm

The EMFlow algorithm is based on a 1D method developed by Macnae and Lamontagne (1987). It was further developed as an industry-standard software package by Macnae et al. (1998). EMFlow employs a fast approximate transformation of AEM data to conductivity estimates of a quasi-layered earth. The data are first deconvolved to a time-constant domain, and then Maxwell's analytic receding-image solution is used to derive independent conductivity and depth values at individual transient decays. Results are then plotted next to each other to produce maps and sections. It is a fast approximate transform that can process large amounts of data in relatively short periods of time, but like all transformation schemes, requires an adequate understanding of the AEM data and the specifications of the acquisition system.

Macnae et al. (1991) present a detailed description of how the conductivity–depth image algorithm was adapted to transform Spectrem data. Comparisons with inversion are shown in following section.

Misfit parameter ϕ_d

The misfit parameter ϕ_d is measure of how well the proposed layered earth models represent the measured survey data at each sounding point. It is a quantitative measure of agreement between the observed data $d^{obs}$and the forward model *f(m),* normalised by the expected error and the number of data as defined in:

$$\phi_d = \frac{1}{N_D}\sum_{k=1}^{N_D}\left(\frac{d_k^{obs} - f(m)}{d_k{}^{err}}\right)^2 \tag{10}$$

$$= [d^{obs} - f(m)]^T W_d [d^{obs} - f(m)]$$

where N_D is the number of data and W_d is diagonal normalization matrix with the level of error for each of data.

Inversions for a 1D earth model assume the conductive properties of the ground are constant, vertically bounded, and remain isotropic throughout each horizontal layer, and the systems' footprint is a spatial constrain. A spatial distribution map of ϕ_d (Figure 7) shows that the inverted models from recorded data can be modelled by a horizontally layered earth in approximately 75% of cases. Values below a limiting threshold of 1.2 ϕ_d, are coloured in cyan. The map highlights areas of low ϕ_d, which are an indication of where higher level of confidence can be expected from the inversion, and models are in better agreement with the observed data.

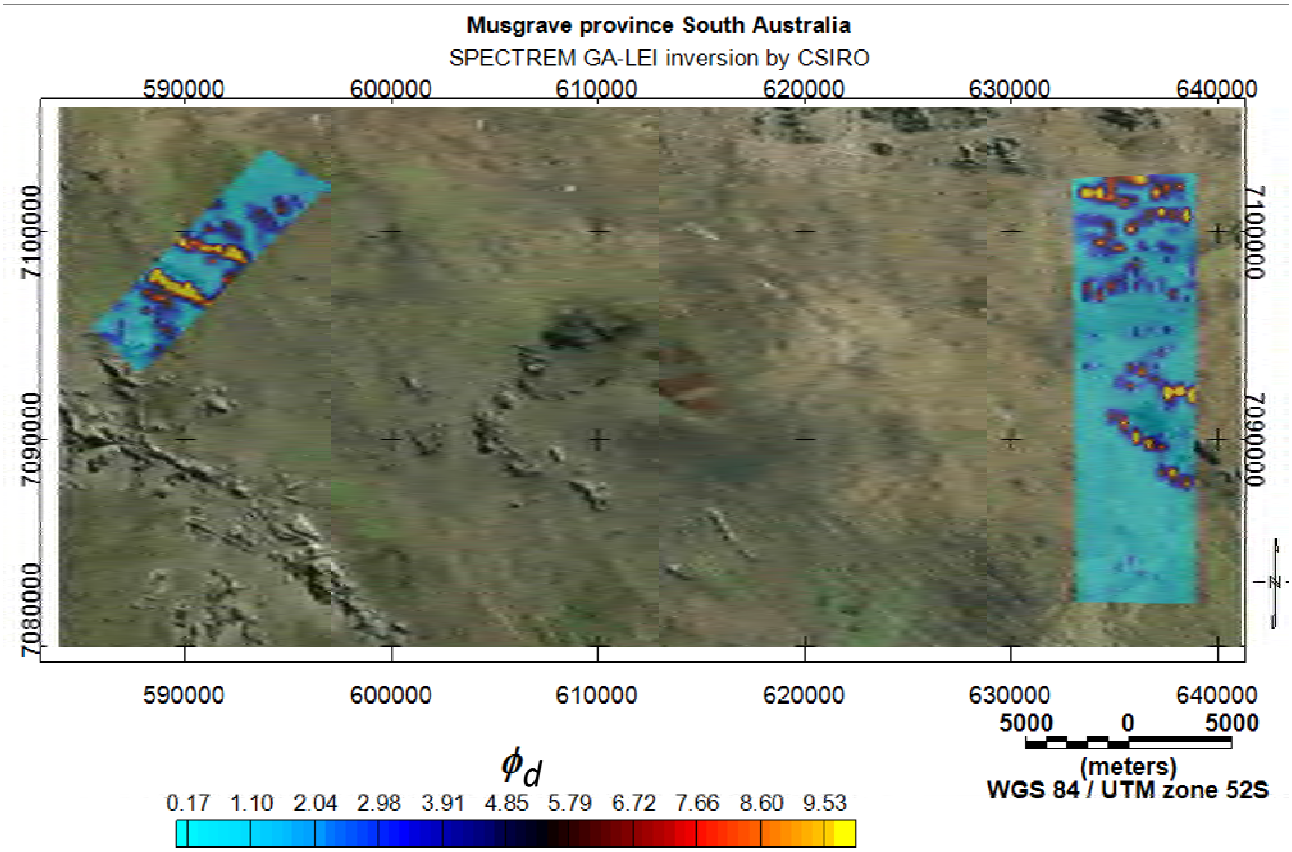

Figure 7. Spatial distribution of parameter ϕ_d draped over an SRTM image. Larger misfit are seen around areas of outcrop and on the margins of depressions filled with sediment.

Further analysis on inversions and transforms

Derived conductivity depth models from AEM data is a routine procedure done by large numbers of contractors using conductivity–depth transforms (CDTs) or layered-earth inversions (LEIs). Most of these algorithms assume a 1D earth model, which may not adequately represent the subsurface. Some important differences between the CDT and LEI approaches identified by Sattel (2005) are:

- CDTs are faster than LEIs (important consideration when inverting thousands of line km).
- CDT transforms rely on accurate depiction of the airborne system geometry, measures that represent a challenge to tracking and monitoring Tx-Rx geometry.
- CDTs do not provide an EM model response, which limits appraisal of the level of fit between derived models and measured data.

In order to assess the data quality, we compare conductivity–depth sections produced with EMFlow, Spectrem Air's in-house software, and the GA-LEI algorithm (Figure 8). Each of these sections appears to recover the same general features, although the GA-LEI inversion better defines structures like shallow layer boundaries in the top 100 m of the profile. All three inversions show some conductivity artefacts (washed-out light blues) that extend to depth (e.g., one about 1400 m from the beginning of the line). Prior experience and other research (Annetts et al., 2000; Ley-Cooper et al., 2010) suggests these are mostly products of edge effects or small, truncated, near-surface conductive bodies, which tend to be imaged deeper greater than their true depths. These artefacts tend to coincide with areas of higher misfit.

The higher definition of the GA–LEI inversion in the near surface (Figure 8 panel C) arguably allows a more accurate interpretation of aquifers, aquitards and other near-surface features that are of interest in understanding regional groundwater resources.

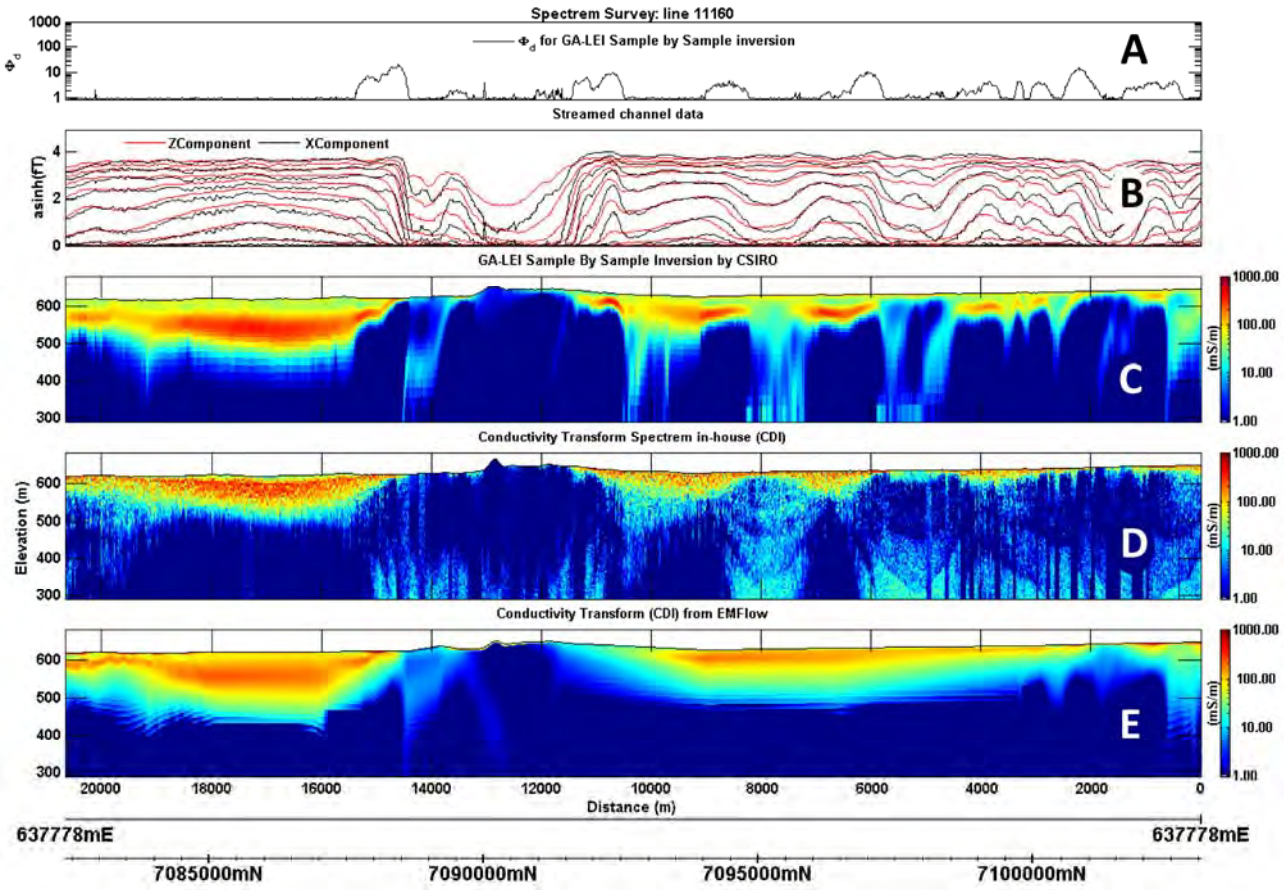

Figure 8. Profiles of line 11160 showing ϕ_d panel A, 10 channels of Z- and X-component measured data panel B, two CDI conductivity–depth sections provided by the Spectrem Air Ltd (panels D and E respectively), and a GA-LEI inverted section (panel C). To allow meaningful comparison, the three conductivity-depth sections are displayed with the same colour scale.

To facilitate easy data comparison and integration purposes, we show different aspects and accompanying measures of AEM data as a multi-plot (Figure 9). The plot facilitates examining the data at its different stages, for quality assurance/control (Qa/Qc) and analysis:

Panel A) shows parameter ϕ_d which is an indicator of how well the proposed 1D layered-earth model represents the measured data at each sounding point.

Panel B) Measured altitude, is a good Qa/Qc indicator of things like weather dependent flying conditions and offcourse elevation changes in the terrain.

Panel C), Nominal-receiver horizontal and Panel D) vertical separations and offsets estimated through primary-field and inversion where plotted to analyse the relative differences amongst them and assess along the flight excursions and find possible spatial relations.

Panel E) The receiver's nominal an inverted attitude is also an indicator of flight stability and a parameter used during the primary-field calculation.

Panel F) Total magnetic intensity, and its correlation to areas of good conductive responses in resistive hosts, is one of the criteria used when determining possible mineral targets.

Panel G) Ten channels of streamed X and Z component data.

Panel H) The inverted sections of conductivity and depth, generated as a second stage product of the process, are displayed with logarithmic colour stretch to show subtle gradual changes and in

Panel I) which shows the same inverted section using a linear colour scale to enhance materials with highly contrasting conductivities.

Areas of resistive ground (deep blue in panels H and I) have less signal and the responses are of lower amplitude (see raw channel profiles, panel G). In areas with suspected sharp boundaries or discontinuous layers, such as at distances of about 580, 1100 and 1470 m from the start of the line, the inversion struggles to fit the data using a horizontal 1D layered model; this is reflected in the lower level of fit indicated by a higher value in ϕ_d (panel A).

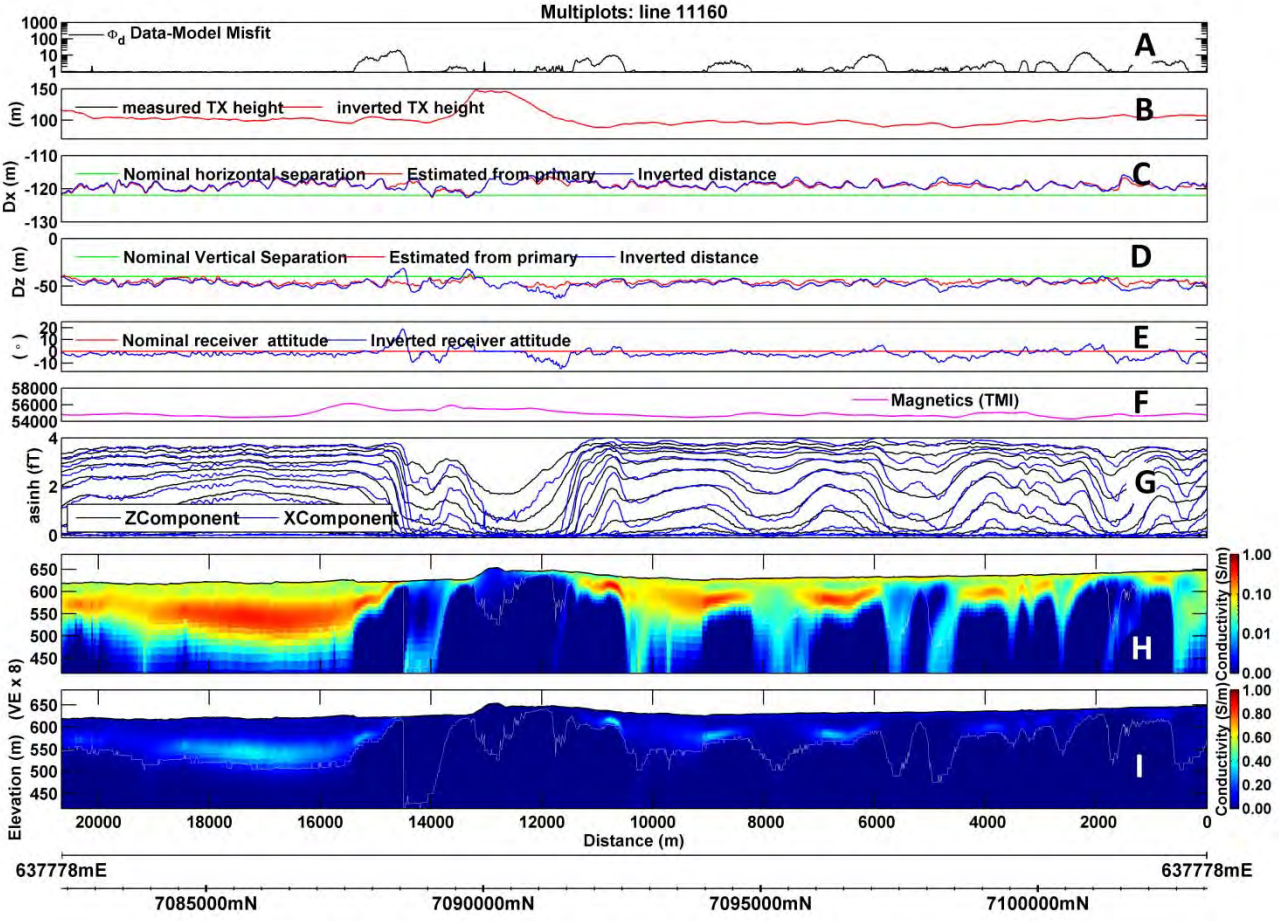

Figure 9. Example of a typical multi-panel plot used for analysis of data and derived inversions (line 11160).

Data misfit

The remote location of the Musgrave Province survey suggests that large inversion misfits are unlikely to be produced by roads, power lines or other man-made sources of noise. Large fitting errors most likely represent responses generated by discontinuities caused by weathering or erosion, plunging bodies, or other abrupt edges such as at faulted boundaries.

Smiarowski et al. (2010) investigated the effects of different flying conditions on the geometry of the recording system. They suggested that the current processing method employed by Spectrem Air retains some level primary-field in the data. This is more prevalent at high frequencies (near surface) and might affect the ability of the system to discriminate shallow targets and is in accordance with the results found in this study (see previous section on Synthetic Modelling). Figure 10 shows measured data along line 11160 and the inverted best fit response from a 1D model. The worst fits occur in the early time channels suggesting that near surface structures would be poorly resolved.

At late times (greater depth), where current has migrated and attenuated, the model plotted in red (predicted data) cannot fit the recorded data, in black (Figure 10).

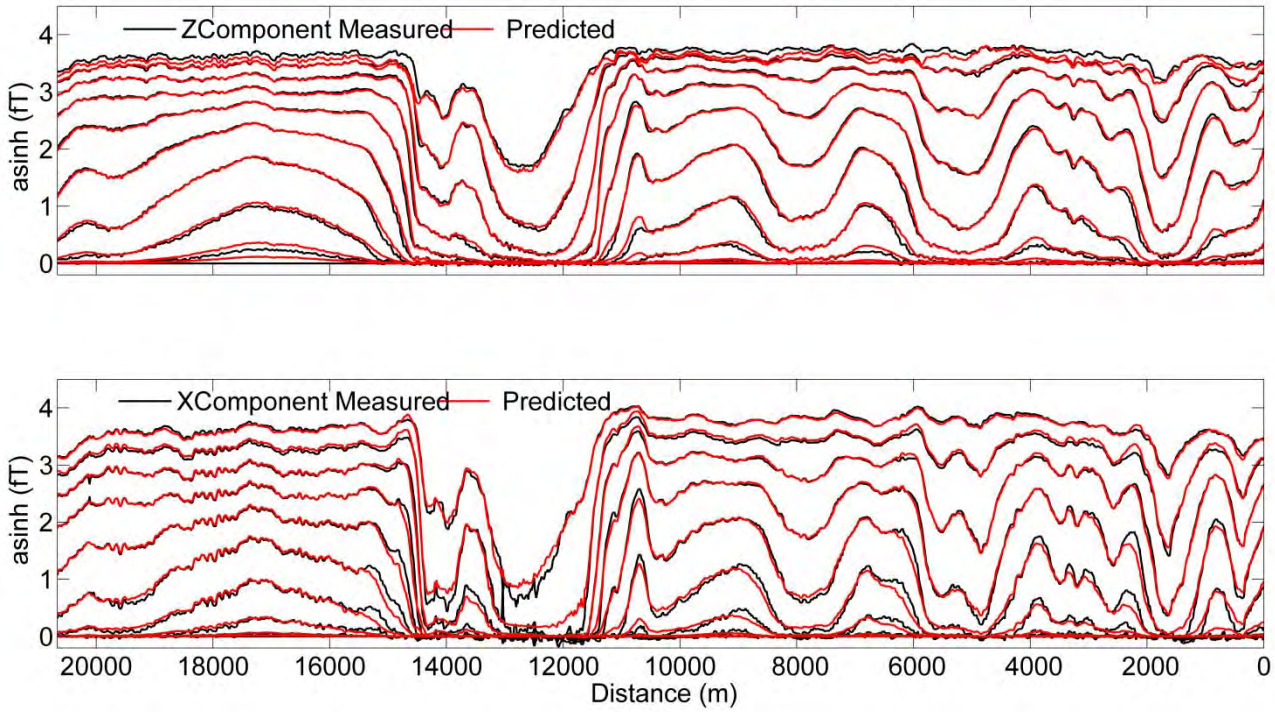

Figure 10 Profile of line 11160 showing 10 channels of X and Z-component measured data (black) and forward-modelled response from best-fit model (red).

The degree of agreement can also be assessed on a sounding-by-sounding basis where each of the 10 windows from both X and Z components of measured data (in grey and black) and the forward responses from a 30-layer model (in red) and a 6-layer model (in blue) are plotted and compared (Figure 11).

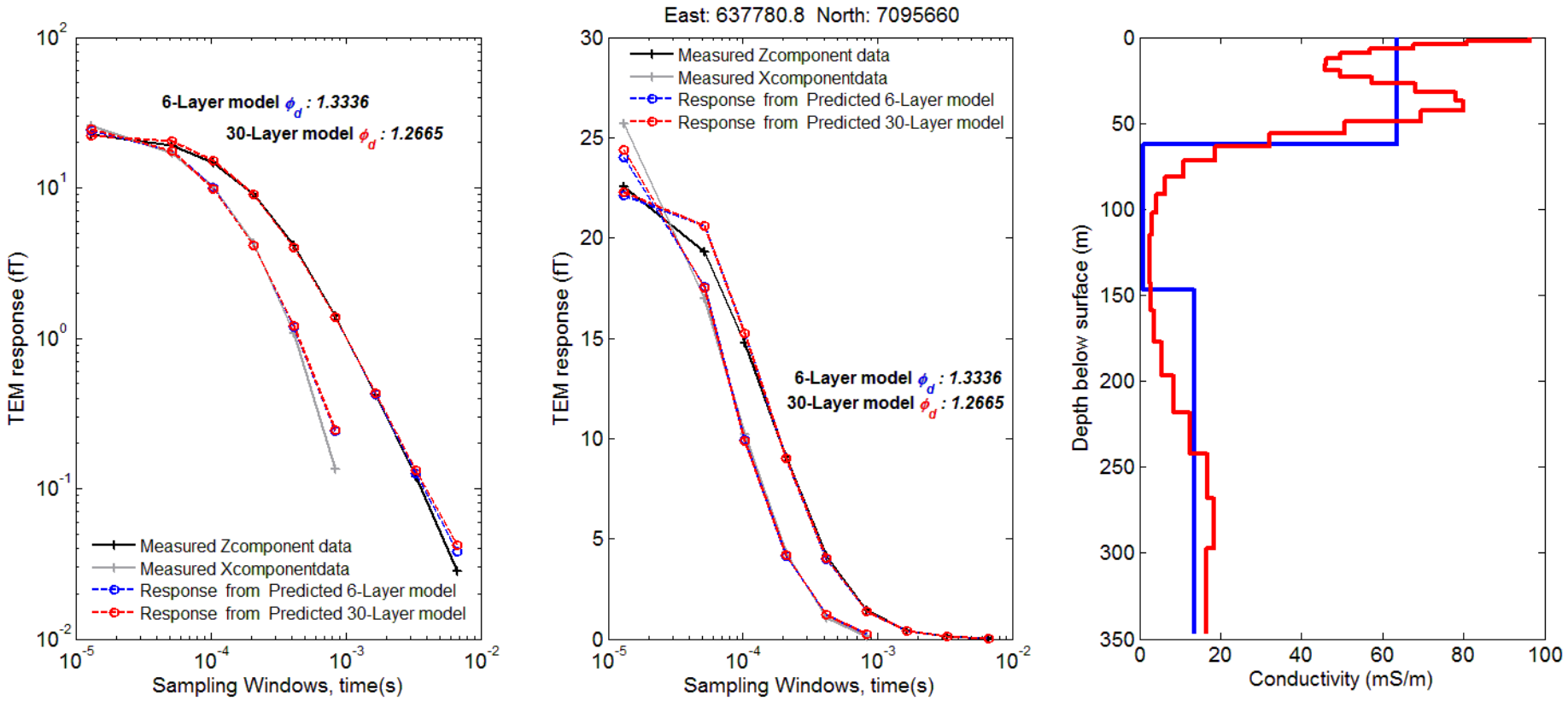

Figure 11. Measured data and predicted responses from a 6-layer and 30-layer inversion, for one sounding. The inversion fails to fit the observed data at early and late times. Left panel plot is on a log-log scale; middle panel log-linear and right panel shows the two proposed conductivity-depth models.

Inversion results and AEM data interpretations

Inversion and processing of SPECTREM data previously described was carried out as part of an analysis of data sets from several systems being employed to develop hydro-geological conceptual models and support groundwater resource assessment in the Musgrave Province of South Australia.

The work involved the reprocessing of historical AEM data sets, including TEMPEST, HoistEM and VTEM. New SkyTEM^{508} and SPECTREM$_{2000}$ data were flown co-incident with TEMEST and VTEM lines. This presents a unique opportunity to assess the different systems over the same terrain and more particularly the results of the inversion approach developed for SPECTREM against inverted data from other systems.

Results for different model parameterisations

For the GA-LEI inversion, the unknowns contained in the model parameter vector to be solved by a 'fixed thickness' inversion process are electrical conductivity for each layer at every location, unmeasured receiver pitch, and Tx–Rx vertical and horizontal separations. We inverted to solve for both a fixed-thickness 30-layer (smooth) model (Figure 12, profile second from bottom) and a 6-layer variable-thickness layer model (Figure 12, bottom profile). The fixed layer thicknesses for the 30-layer model are shown in Table A3. 1 in Appendix III. For the variable-thickness inversion, both layer thickness and conductivity were inverted for. To enforce positive conductivity values, the algorithm inverts for logarithms of the conductivities assigned to each layer.

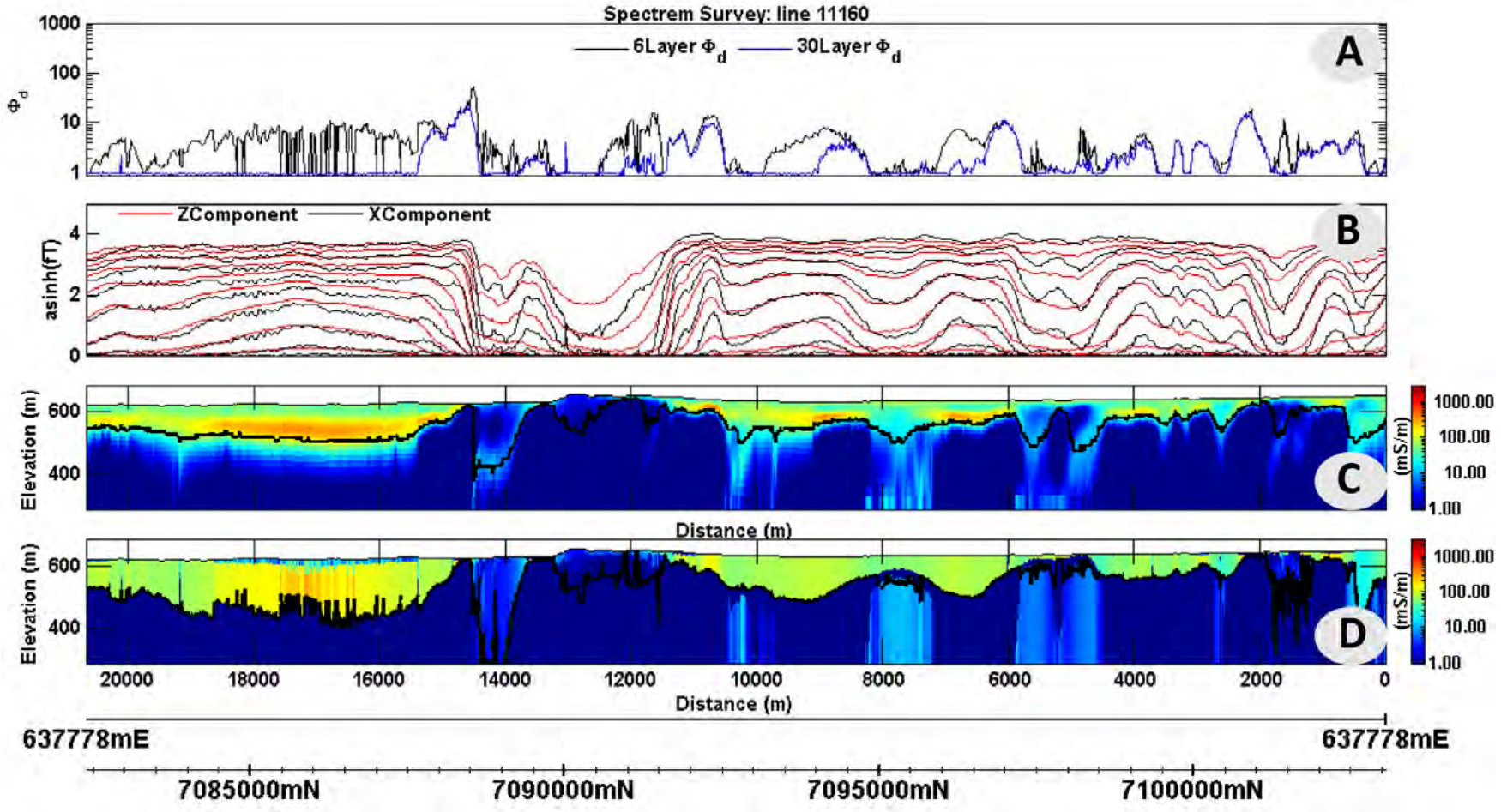

Figure 12. Line 11160 of SPECTREM data from the Musgrave province survey. Panel A shows how the data can be represented by a 1D model (parameterϕ_d). Panel B shows processed channel X- and Z-component data. Panel C shows a 30-layer inversion with fixed layer thicknesses. Panel D shows a 6-layer inversion where both conductivities and layer thicknesses are solved by inversion.

Airborne EM data which have been inverted or transformed to show variation of conductivity with depth can be plotted as sections or maps for a quantitative and more visually intuitive way of looking at data which can then be utilized in the mapping interpretation of geological materials.

Three images of conductivity-depth intervals of 114 to 126 m, 49 to 56 m and 0 to 2m (Figure 13, Figure 14 and Figure 15) detail the structure of bodies that share common geo-electrical properties and the extension of those features with depth. For example, in the eastern part of Figure 13 a northwest–southeast trending conductive body is clearly defined between 114 and 126 m depth. This feature follows the edge of an outcropping resistive ridge and might be associated either with an aquifer containing highly saline water or a natural depression filled with clay-rich sediment.

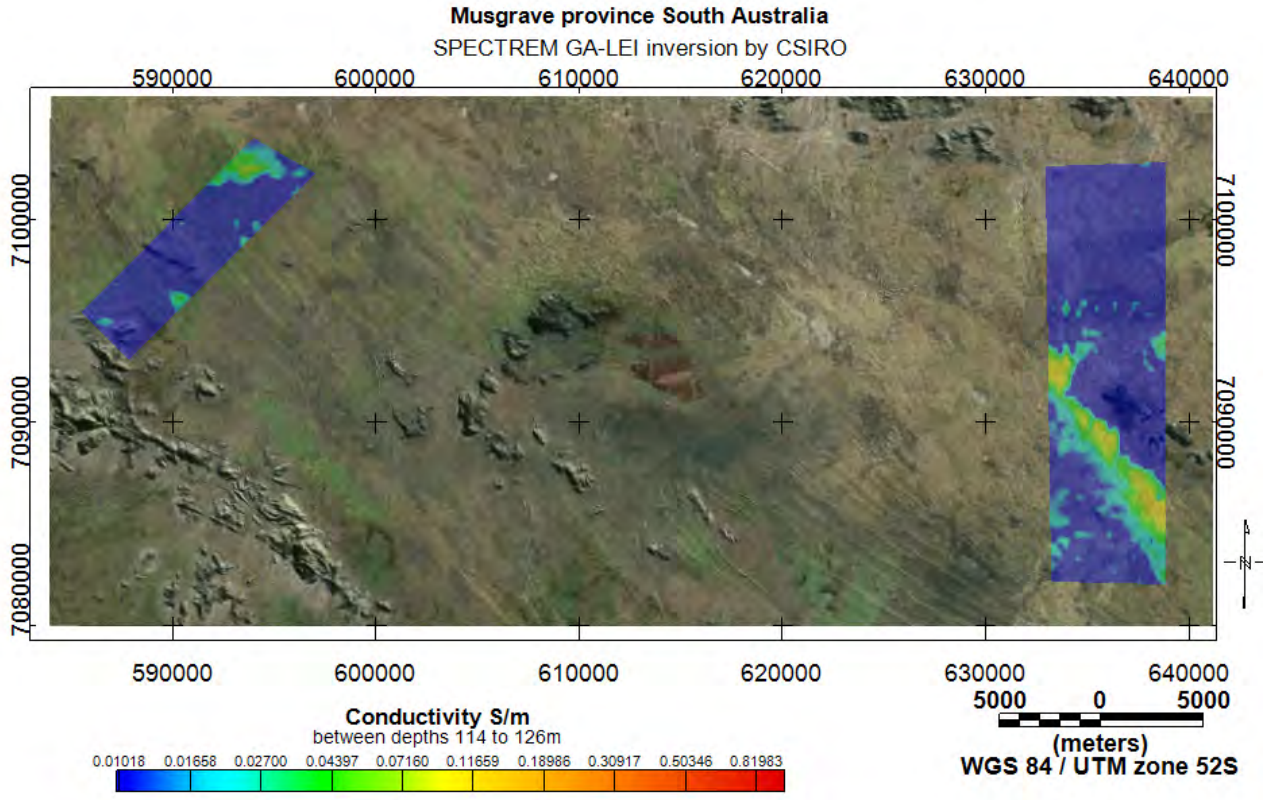

Figure 13. Conductivity–depth interval from 114 to 126 m below the surface.

The edge of the northwest–southeast trending resistive ridge defined at 114–126 m (Figure 13) is also evident at 49–56 m depth (Figure 14), but its southwest border is masked by a lack of contrast with the conductivity of surrounding material. The very near surface map (0–2 m, Figure 15) again shows the presence of the aforementioned conductive feature but, in contrast to the 49–56 m slice, it defines the southwest boundary.

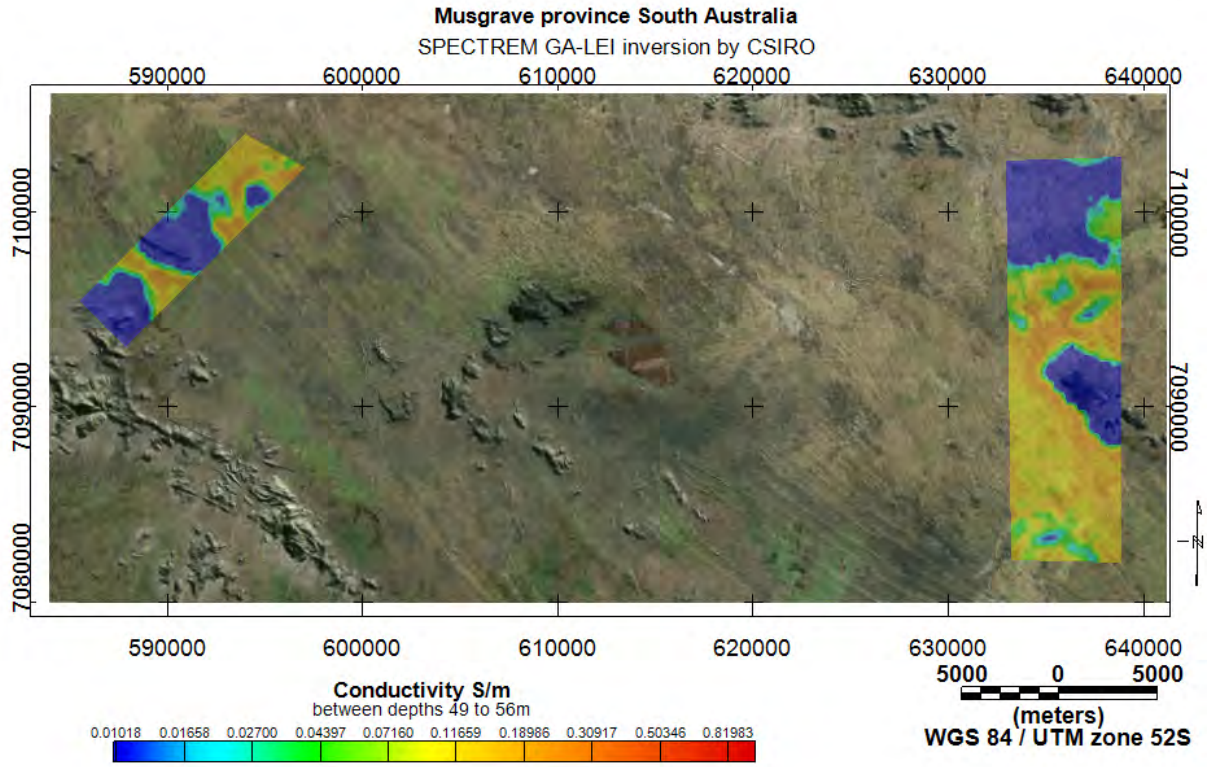

Figure 14. Conductivity–depth map from 49 to 56 m below the surface.

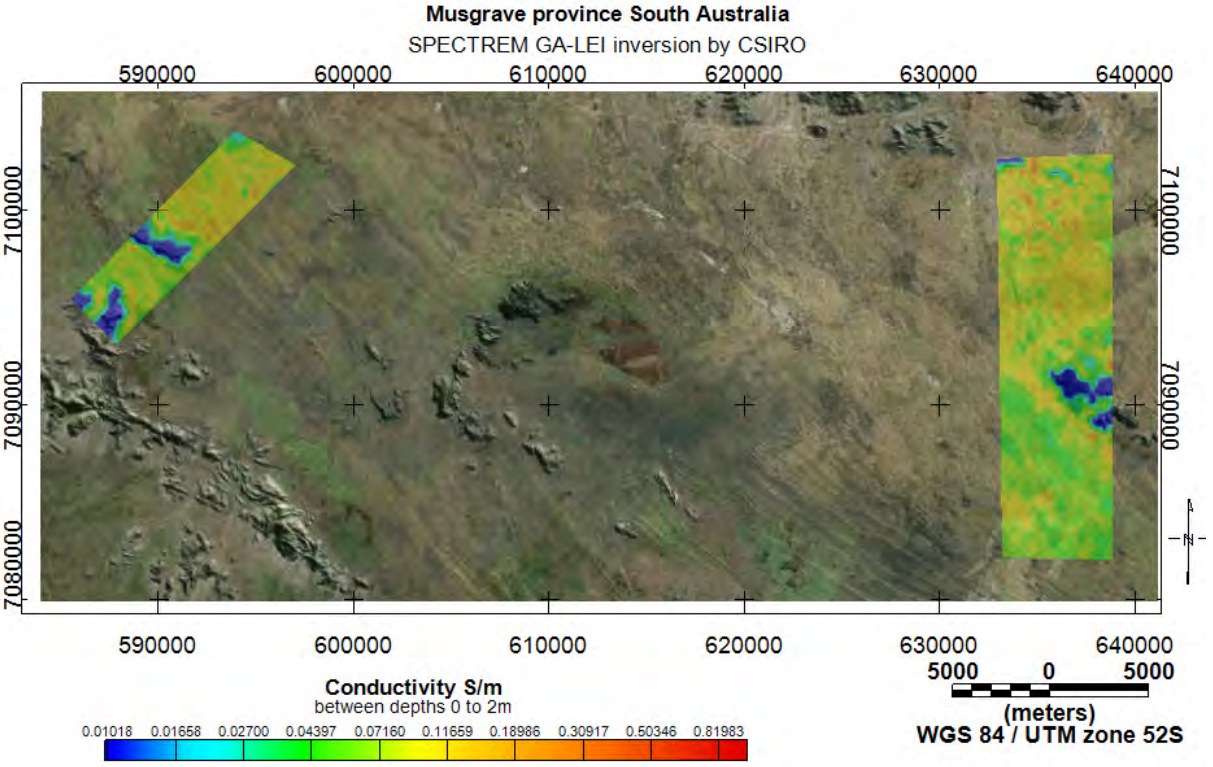

Figure 15. Conductivity–depth range, from 0 to 2 m below the surface.

Comparison of AEM systems

A helicopter-borne VTEM survey was flown in 2011 over previously acquired (1998) TEMPEST data. SPECTREM and SkyTEM data acquired over the same data with a similar orientation in 2012 and present an opportunity to compare the acquisition systems, inversion algorithms, and to better understand the hydrogeology of the surveyed area.

A comparison of these systems (Figure 16) is shown by 30-layer inversions over the four coincident profiles. There are subtle differences in the features resolved by each system, for example, a feature 1000 m from the beginning of the line that was resolved only by the SkyTEM low-moment (LM) and SPECTREM systems. This feature may represent a decrease of ground water salinity between an upper conductive layer and an underlying clay layer. Resolution of these shallow layers is an interesting comparison point; since the SkyTEM LM has been designed to fly low, turn-off fast and resolve near surface features (Sørensen and Auken, 2004), whilst the SPECTREM's ability to resolve near surface features resides on the shape of its wave-form and its on-time measurements (as discussed previously in the System description section).

All of the conductivity–depth sections produced by inversion of the SPECTREM data (Figure 16) resolve structures similar to those that other EM systems have previously resolved in the survey area, including structures of hydrogeological interest such as sediment-filled palaeovalleys.

A comparison of inversion models from two individual soundings S1 and S2, of the SPECTREM, VTEM and TEMPEST data along coincident lines is shown in Figure 17. The two sounding show recovered models from all system over areas of predominantly conductive (S1) and mostly resistive ground (S2). For sounding S1 on the left the SPECTREM data shows a conductive cap layer that was not detected by TEMPEST or VTEM. This feature is yet to be corroborated by ground-truthing.

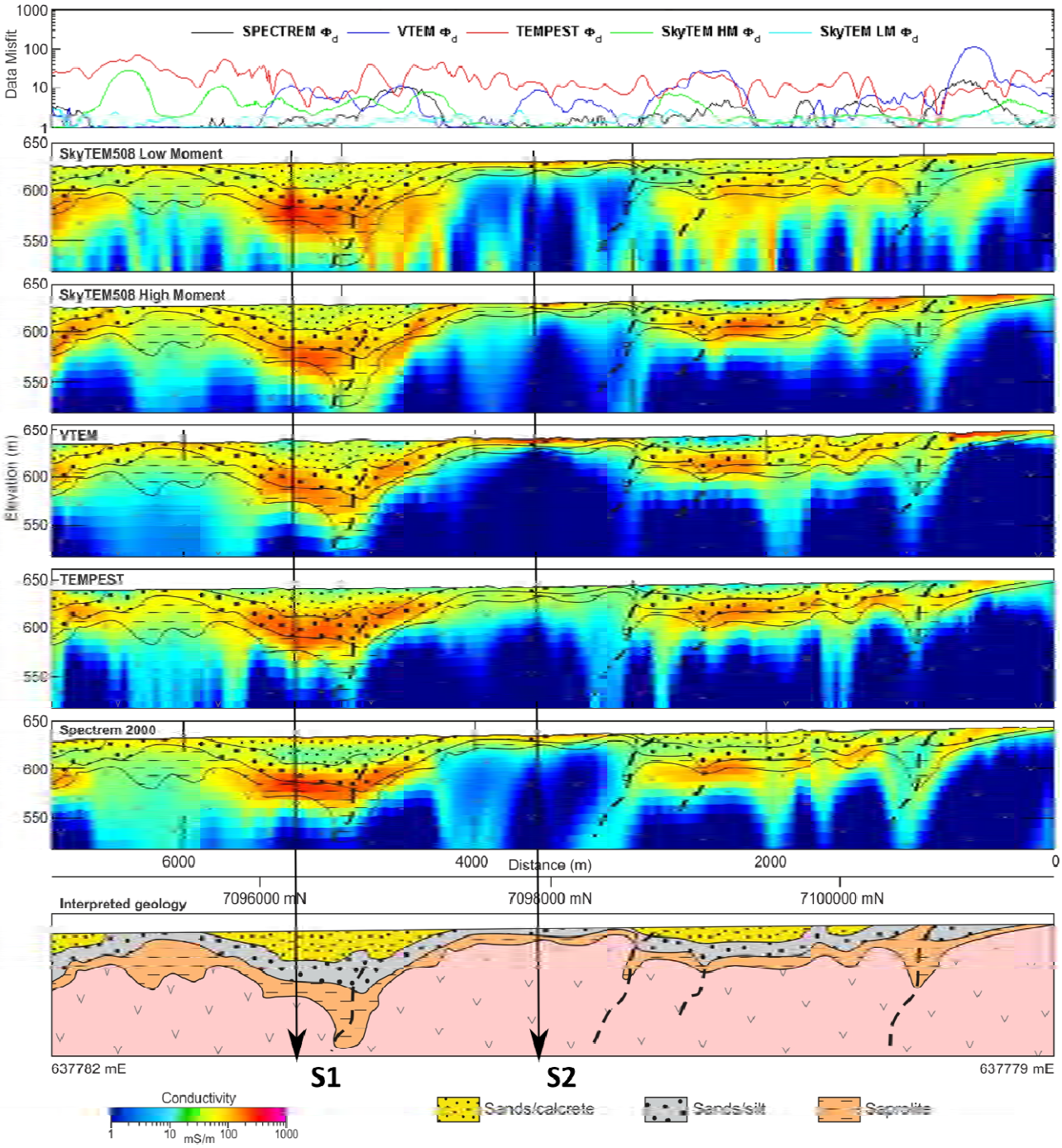

Figure 16. Comparison of 30-layer inversions of four coincident north–south lines flown in 1998, 2011 and 2012 using Tempest, VTEM, SkyTEM^{508} and SPECTREM$_{2000}$AEM systems. Interpreted geology (from limited off-section drilling) is superimposed.

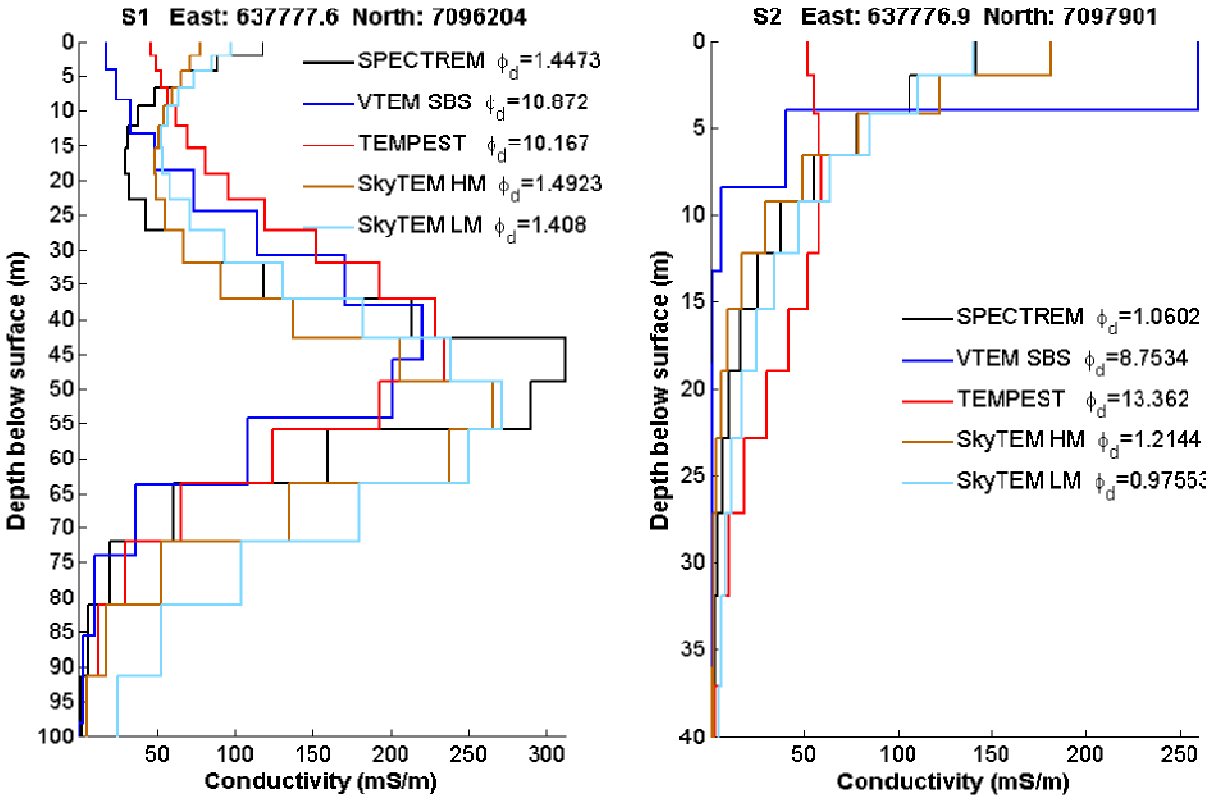

Figure 17. Comparisons of individual soundings for SPECTREM, VTEM , TEMPEST and SkyTEM data at two locations along coincident lines after inversion with the 30-layer starting model for the GA-LEI inversion. The two soundings show recovered models from all system over conductive and resistive area.

The overall best fits were achieved with the SkyTEM low-moment data, followed by the SPECTREM data in Table 2 and Table 3. Table 3 needs to be analysed carefully, as results on the statistics can be deceptive, since the areas flown by the different systems do not cover the exact same extents and were flown at very different periods of time (SPECTREM and SkyTEM in 2012 , VTEM in 2011 and TEMPEST in late 1999).

The mapped areal distribution of ϕ_d (Figure 7) shows that the inverted models yielded by the recorded SPECTREM data can be represented by a horizontally layered-earth (considering 1.2 ϕ_d as threshold) with a reasonable degree of accuracy in close to 75% of cases.

Both fixed-wing systems (SPECTREM and TEMPEST), have used X and Z components have been used in the inversion, whilst only the Z component has been used for the helicopter-borne systems. The TEMPEST data did not include system geometry, so Tx–Rx separations are unknown and were not included in the inversion. The discussion in System geometry and its implications section of this report suggests that the omission of the system geometry may have compromised the inversion's fitting of the data. For the VTEM data, we needed to omit the first three data channels in order to achieve a reasonable fit to the early time channels. The omission of these three channels from the inversion has clearly hindered the VTEM's resolution of the near surface. We are also aware that combining the SkyTEM low- and high-moment data would improve the system's vertical coherency.

Table 2. ϕ_d values for four systems over the coincident line shown in Figure 16.

	Minimum	Maximum	Mean	Std dev.	No. of points
SPECTREM	0.8782	15.8160	2.5505	2.76596	562
TEMPEST	0.9558	69.3530	17.8528	12.7199	529
VTEM	0.7068	114.9000	7.9850	16.7442	529
SkyTEM HM	0.8732	28.0490	3.47879	4.34376	2978
SkyTEM LM	0.9424	3.0368	1.36616	0.42677	2978

Table 3 Whole of survey ϕ_d values for the four systems used in the Musgrave Province.

	Minimum	Maximum	Mean	Std dev.	No. of points
SPECTREM	0.51085	159.11000	2.30411	3.58936	44576
TEMPEST	0.8930	205.2400	24.4423	19.0287	16078
VTEM	0.33057	570.62000	24.25489	57.23154	35136
SkyTEM HM	0.21177	322.97000	3.47956	7.10705	16366
SkyTEM LM	0.47779	14.88700	1.45296	0.58325	15985

Conclusions

Through inverted SPECTREM data for the Musgrave Province, we show that the conductivity-depth models can be used to define the extent, geometry and depth of regional palaeovalleys aquifers, thus helping in the conceptualisation of the regions' hydrogeology and groundwater resources. Geoscience Australia's LEI algorithm was used to individually invert each sounding of the SPECTREM survey data, solving for conductivity, receiver pitch, vertical and horizontal Tx–Rx separations and, in some cases layer thickness. This approach yielded quantitative information about the subsurface conductivity and resolved conductivity–depth structures similar to those previously obtained from other AEM systems.

The process of inverting the SPECTREM data has provided us with a better understanding of the capabilities and performance of this particular airborne EM system. High-altitude data and synthetic forward models were analysed to understand the system's noise levels, and to evaluate its effectiveness for mapping geology with contrasting conductivities in the presence of conductive (1 S/m) overburden, which is common in South Australia. By considering different approaches to primary field removal, methods of data normalization, and understanding Tx–Rx geometry, we have developed a procedure to quantitatively model and invert SPECTREM data. Although Tx–Rx separations are not routinely monitored in flight by Spectrem Air, they can be estimated during data processing. If Tx–Rx separations are not properly taken into account, the early time responses are those most affected, hindering the system's ability to resolve near-surface features. The results presented here demonstrate the value of accurate system characterisation in better defining variability in the subsurface that might represent variation in aquifer character of groundwater quality, or both.

The analyses of data processed and transformed by various algorithms showed that although all of them resolved the same general features, results from the inversion better defined subtle features in the uppermost 100 m of the profile. This higher level of definition is important for interpretation of potential aquifers, aquitards and near-surface features of interest in understanding regional hydrogeology.

It is important to note that our interpretation of the inverted SPECTREM AEM data would benefit from application to larger data sets. The work described here has focused on identifying and quantifying uncertainty in both data acquisition and processing procedures to deliver subsurface interpretations of greater certainty.

Inversion results by their very nature remain ambiguous. The comparison of the GA-LEI and other inversion algorithms, and of different acquisition systems, does not necessarily advocate the use of a particular inversion procedure, or a particular acquisition system. They show that there are equally valid ways of both sounding the subsurface and interpreting the results, and that the optimum approach may be dependent on local geological or hydrogeological conditions.

References

Annan, A. P., (1986), Development of the Prospect I Airborne ElectroMagnetic System: Airborne Resistivity Mapping,Geological Survey of Canada, Paper no. 86-22, 63-70.

Annetts, D., Sugeng, F., Macnae, J., and Raiche, A., (2000), Modelling the airborne electromagnetic response of a vertical contact: Exploration Geophysics, 31(2), 115-125.

Auken, E., and Christiansen, A. V., (2004), Layered and laterally constrained 2D inversion of resistivity data: Geophysics, 69(3), 752-761.

Boyd, G. W., (2004), HoistEM--A new airborne electromagnetic system: PACRIM Proceedings.

Brodie, R. C. (2009), A holistic approach to the calibration, processing and inversion of airborne electromagnetic data, Ph.D. thesis, Australian National University, Canberra.

Brodie, R. C. (2010), Holistic Inversion of Airborne Electromagnetic Data, PhD thesis, 305 pp, The Australian National University.

Brodie, R. C., (2012), Appendix 3: GA-LEI Inversion of TEMPEST Data, in The Frome airborne electromagnetic survey, South Australia: implications for energy, minerals and regional geology. edited by I. C. Roach, pp. 278-287, Geoscience Australia Record 2012/40-DMITRE Report Book 2012/00003.

Christiansen, A. V., Auken, E., and Viezzoli, A., (2011), Quantification of modeling errors in airborne TEM caused by inaccurate system description: Geophysics, 76(1), F43-F52.

Constable, S. C., Parker, R. L., and Constable, C. G., (1987), Occam's inversion; a practical algorithm for generating smooth models from electromagnetic sounding data: Geophysics, 52(3), 289-300.

Cox, L. H., Wilson, G. A., and Zhdanov, M. S., (2010), 3D inversion of airborne electromagnetic data using a moving footprint: Exploration Geophysics, 41(4), 250-259.

Davis, A. C., and Macnae, J., (2008), Quantifying AEM system characteristics using a ground loop: Geophysics, 73(4), F179–F188.

Farquharson, C. G., and Oldenburg, D. W., (1996), Approximate sensitivities for the electromagnetic inverse problem: Geophysical Journal International(126), 235-252.

Farquharson, C. G., Oldenburg, D. W., and Routh, P. S., (2003), Simultaneous 1D inversion of loop-loop electromagnetic data for magnetic susceptability and electrical conductivity: Geophysics, 68(6), 1857-1869.

Green, A., and Lane, R., (2003), Estimating Noise Levels in AEM Data: ASEG 16th Geophysical conference and exhibition, Extended abstracts.

Klinkert, P. S., Leggatt, P. B., Huge, T. B., and Biesheuvel, K., (1996), SPECTREM airborne electromagnetic system — current status and performance, paper presented at SEG Technical Program Expanded Abstracts 1996.

Klinkert, P. S., Leggatt, P. B., and Hage, T. B., (1997), The Spectrem airborne electromagnetic system – latest developments and field examples, paper presented at Fourth International Conference on Mineral Exploration.

Lane, R., Green, A., Golding, C., Owers, M., Pik, P., Plunkett, C., Sattel, D., and Thorn, B., (2000), An example of 3D conductivity mapping using the TEMPEST airborne electromagnetic system: Exploration Geophysics, 31, 162-172.

Lane, R., Brodie, R. C., and Fitzpatrick, A.,(2004), Constrained inversion of AEM data from the Lower Balonne area, Southern Queensland, Australia.Cooperative Research Centre for Landscapes, Environment and Mineral Exploration *Open file report 163*.

Leggatt, P., and Pendock, N., (1993), Conductivity-depth imaging of airborne electromagnetic step-response data using maximum entropy: in Mohammad-Djafari, A. and Demaments, C., Eds., Maximum entropy and Bayesian methods, Kluwer Acad. Publ., 281-286.

Leggatt, P. B., Klinkert, P. S., and Hage, T. B., (2000), The Spectrem airborne electromagnetic system—further developments: Geophysics, 65(6), 1976-1982.

Ley-Cooper, Y., Macnae, J., and Viezzoli, A., (2010), Breaks in lithology: Interpretation problems when handling 2D structures with a 1D approximation: Geophysics, 75(4), WA179-WA188.

Liu, G., (1998), Effect of transmitter current waveform on airborne TEM response: Exploration Geophysics, 29 (1 & 2), 35-41.

Macnae, J., and Lamontagne, Y., (1987), Imaging quasi-layered conductive structures by simple processing of transient electromagnetic data: Geophysics, 52(4), 545-554.

Macnae, J., Smith, R., Polzer, B. D., Lamontagne, Y., and Klinkert, P. S., (1991), Conductivity-depth imaging of airborne electromagnetic step-response data: Geophysics, 56(1), p. 102-114.

Macnae, J., King, A., Soltz, N., Osmakoff, A., and Blaha, A., (1998), Fast AEM data processing and inversion: Exploration Geophysics, 29, p. 163-169.

Pare, P., Gribenko, A. V., Cox, L. H., Čuma, M., Wilson, G. A., Zhdanov, M. S., Legault, J., Smit, J., and Polome, L., (2012), 3D inversion of SPECTREM and ZTEM airborne electromagnetic data from the Pebble Cu–Au–Mo porphyry deposit, Alaska: Exploration Geophysics, 43(2), 104-115.

Polzer, B. D. (1985), The interpretation of inductive transient magnetic sounding data, M.Sc thesis, University of Toronto.

Reid, J. E., and Vrbancich, J., (2004), A comparison of the inductive-limit footprints of airborne electromagnetic configurations: Geophysics, 69(5), 1229-1239.

Sattel, D., (1998), Conductivity information in three dimensions: Exploration Geophysics, 29(1&2), 157-162.

Sattel, D., (2005), Inverting airborne electromagnetic (AEM) data with Zohdy's method: Geophysics, 70(4), G77-G85.

Smiarowski, A., Macnae, J., and Bailey, R. C., (2010), Predictive filter calculation of primary fields in a fixed-wing time-domain AEM system: Geophysics, 75(4), F97-F106.

Smith, R., (1998), On the effect of varying the pulse width to detect high conductance bodies: Exploration Geophysics, 29 (1 & 2), 42-45.

Smith, R., (2001a), On removing the primary field from fixed-wing time-domain airborne electromagnetic data: some consequences for quantitative modelling, estimating bird position and detecting perfect conductors: Geophysical Prospecting, 49(4), 405-416.

Smith, R. S., (2001b), On removing the primary field from fixed–wing time–domain airborne electromagnetic data: some consequences for quantitative modelling, estimating bird position and detecting perfect conductors: Geophysical Prospecting, 49, 405–416.

Smith, R. S., (2001c), Tracking the transmitting-receiving offset in fixed-wing transient EM systems: methodology and application: Exploration Geophysics, 32(1), 14-19.

Smith, R. S., and Neil, B., (2012), Precision requirements for specifying transmitter waveforms used for modelling the off-time electromagnetic response: Exploration Geophysics, -.

Sørensen, K., I., and Auken, E., (2004), SkyTEM; a new high-resolution helicopter transient electromagnetic system: Exploration Geophysics, 35(3), 194-202.

Sørensen, K. I., and Auken, E., (2003), New developments in high resolution airborne TEM instrumentation: ASEG Extended Abstracts, 2003(2), 1-4.

Viezzoli, A., Christiansen, A. V., Auken, E., and Sorensen, K., (2008), Quasi-3D modeling of airborne TEM data by spatially constrained inversion: Geophysics, 73(3), F105-F113.

Wait, J. R., (1982), Geo-electromagnetism, 268 pp., Academic Press Inc, New York.

Witherly, K., Irvine, D., and Morrison, E., (2004), The Geotech VTEM time domain helicopter EM system: 74th Annual International Meeting, SEG, Expanded Abstracts, 1217-1220.

Worrall, L., Munday, T., and Green, A., (1998), Beyond bump finding - airborne electromagnetics for mineral exploration in regolith dominated terrains: Exploration Geophysics, 29 (1 & 2), 199-203.

Appendix I: Standard report by Spectrem Air

By Phil Klinkert, Jaco Smit, Louis Polomé and Nirocca Devkurran

Basic survey parameters

Base of operations	Ayers Rock (Australia)
Flying dates	9 April 2012
Survey type	Electromagnetic, magnetic, radiometric, terrain
Aircraft type	DC3 – TP67
EM base Frequency	25 Hz
Nominal aircraft altitude	90 m
Nominal aircraft speed	60 m/s
Acceptable kilometres flown:	351 line kilometres
Nominal flight-line spacing	300 m
Nominal flight-line direction:	0 degrees
Nominal tie-line spacing	n/a
Nominal tie-line direction:	n/a

Datum

All coordinates provided in processed digital data-sets have the following datum parameters.

Datum	WGS 84
Projection	UTM Zone 52S

Survey area coordinates

Area coordinates	Easting (m)	Northing (m)
(entire area)	633079	7083199
	633079	7101448
	638890	7101447
	638890	7083198
	633079	7083199

System specifications

The SPECTREM system simultaneously takes electromagnetic, total field magnetic and radiometric measurements. Both the electromagnetic and magnetic sensors are towed behind the aircraft in "birds". Radiometric crystals are installed inside the aircraft cabin. The geometry of the system and other system specifications are listed below.

EM system

Transmitter height above	91 m
Tx–Rx vertical separation	41 m (nominal value)
Tx–Rx horizontal separation	121 m (nominal value)
Transmitter coil axis	Vertical
Receiver coil axes	X : horizontal, parallel to flight direction; Z: vertical
Current waveform	Square wave
Base frequency	25 Hz
Transmitter loop area	420 m^2
RMS current	960 A
RMS dipole moment	400 000 Am^2
Digitising rate @ 25Hz	38 400 Hz/component
Recording Rate	5 Hz
Number of windows	9 per component
Window distribution	Pseudo-binary
Window times 25 Hz	

Window number	Start (ms)	End (ms)	Centre (ms)	Width (ms)
1	0.0260	0.0260	0.0260	0
2	0.0521	0.0781	0.0651	0.0260
3	0.1042	0.1823	0.14325	0.0781
4	0.2083	0.3906	0.29945	0.1823
5	0.4167	0.8073	0.6120	0.3906
6	0.8333	1.6406	1.23695	0.8073
7	1.6667	3.3073	2.4870	1.6406
8	3.3333	6.6406	4.98695	3.3073
9	6.6667	13.3073	9.9870	6.6406
10 (Primary field)	13.3333	19.9740	16.6536	6.6667

Magnetic system

Bird height above ground	72 m
Bird location	19 m below and 41 m behind centre of aircraft
Sensor	Scintrex CS-2 Sensor with SPECTREM Counter
Recording rate	5 Hz
Sensitivity	0.01 nT
Resolution	0.1 nT

Positioning system

Sensor	Novatel RT-20 GPS receiver with Fugro Omnistar differential
Recording rate	5 Hz

Other sensors	
Radar altitude	Collins with 5 Hz sampling with 0.3 m resolution
Laser altitude	Riegl with 5 Hz sampling with 0.03 m resolution
Barometric pressure	Rose Mount with 1 Hz sampling
Temperature (OAT)	PT-100 RTD with 1 Hz sampling
Analogue chart recorder	RMS GR-33

Data Processing

Electromagnetic Processing

Aircraft Processing

Some of the most important EM data processing was carried out on the aircraft as it acquired the data. The first processing stage was stacking the data to 512 samples. The data was then deconvolved to remove system response and transformed to a square wave. A square transmitter waveform was chosen as a periodic approximation of the step response.

In the next stage of processing the data was binned into 8 channels or windows. As the SPECTREM system makes its measurement while the transmitter is switched on, it is necessary to separate the primary (transmitted) field from the (induced) secondary field. The assumption is made that the induced field will have decayed to a minimal amount at the time the last channel is sampled. As the last channel measures only the primary field, it can be subtracted from the other channels to separate the secondary field. Hence, there are actually 8 channels with geological information in the final data.

Profile data

The spikes in the line data have been removed using a 3-point Naudy filter. The line data have also been drift corrected and micro-levelled. The drift is particularly noticeable on the later time channels and has been applied to channels 4 to 8. This is an iterative process, with the assumption that there is a constant drift on a single line. This is reasonable if the lines are short. The processing steps are:

The channel data are clipped retaining the data in the resistive areas where the response should be close to zero.

The average of the clipped data is then calculated and subtracted from the channel data.

The steps are then repeated, refining the correction.

Decorrugation and micro-levelling have been applied to all the channels to reduce small residual errors that have not been corrected through the drift correction method.

Apparent Conductivity

The apparent conductivity was calculated from its channel amplitudes and the aircraft height. An apparent conductivity is the conductivity of a half space that would produce an amplitude equivalent to the

measured response. It is useful in providing a physically sensible unit and partially compensates for aircraft ground clearance variations. The unit for apparent conductivity is milliSiemens per metre (mS/m).

Magnetic Processing

Levelling processing included:

Tie-line levelling

Decorrugation

Micro-levelling.

Tie-line Levelling

Tie line levelling is used to remove the diurnal variation and errors due to instrument drift; both are assumed to vary slowly over time.

Tie-line levelling is an iterative process:

Calculate the mis-closures at the crossover points of the tie and traverse lines. The mis-closure is the difference between the magnetic value on the tie line and the traverse line. The mis-closures are weighted by the gradient of the total field at the crossover point.

$$Weight = 1 / e^{(0.1 \times gradient)}$$

The error is approximated by a piecewise polynomial as a function of time along a flight line and then along a tie line. These steps are repeated until a good fit has been obtained.

Decorrugation

This is a grid based operation designed to reduce the residual errors that the tie-line levelling does not remove. These are due to inaccuracies in the crossovers, localised diurnal activity, and local altitude variations.

Elongated anomalies with the following characteristics are removed:

2 times the line spacing perpendicular to the line direction

2 times the tie line spacing parallel to the line direction

small dynamic range

Micro-levelling

Applies the corrections made to the grid to the profile data and thereby enhances the line data by removing the final residual errors. The micro-levelled data are then gridded. The lag correction is 40 m.

DEM processing

Initially, the GPS height and the radar altimeter channels are visually inspected and any spikes or discontinuities are removed. A Low Pass or Naudy Filter is then applied to both channels. The GPS height channel is then gridded and the resultant grid is checked. Due to the nature of the GPS data, it is normally necessary at this stage to perform some degree of decorrugation on the grid with the corrections then written back to the database.

The radar altimeter channel is then subtracted from the corrected GPS height channel in the database and the resultant channel is gridded and verified.

Radiometric Processing

The processing of the radiometric data uses the full 256 channel spectra for most of the corrections. This processing allows us to use the information from the full spectrum to enhance the regions of interest in the spectrum, namely, Potassium, Uranium and Thorium.

Appendix II: GA-LEI SBS Inversion of SPECTREM$_{2000}$ Data

Adapted from Brodie (2012) with permission.

Introduction

The GA-LEI inversion program is capable of inverting data from most airborne time-domain AEM systems. It has the capability of inverting for layer conductivities, layer thicknesses, and system geometry parameters, or some subset of these. There are options to use a multi-layer smooth-model formulation (Constable et al., 1987) or a few-layer blocky-model formulation (Sattel, 1998). For the sake of simplicity, only the aspects of the algorithm that are relevant to the inversion of SPECTREM data using a multi-layer smooth-model are described here.

SPECTREM data consist of a collection (tens of thousands to millions) of point located multi-channel samples acquired at 0.2s (approximately 15m) intervals along survey flight lines. The algorithm independently inverts each sample. The data inputs to the inversion of each sample are the observed total (primary plus secondary) field X-component and Z-component data. Auxiliary information input into the algorithm are the measured and assumed elements of the system geometry, the thicknesses of the layers, and prior information on the unmeasured elements of the system geometry and ground conductivity. The unknowns solved for in the inversion (outputs) are the electrical conductivity of the layers and the unmeasured elements of the system geometry.

Since each sample is inverted independently, the user may elect to invert all samples or some subset of them. The inversion of each sample results in an estimate of a one dimensional (1D) conductivity structure associated with that sample. Each estimated 1D conductivity structure, although theoretically laterally constant and extending infinitely in all directions, is only supported by the data within the system footprint centred about the sample point (Reid and Vrbancich, 2004). So by progressively inverting all the samples and stitching together the resultant 1D conductivity structures a depiction of the overall laterally variable 3D conductivity structure is built up.

Formulation

Figure 2 shows the overall framework under which the inversion of a single airborne sample is carried out. The elements of the figure are progressively described in the following sections.

Coordinate system

Since each sample is inverted separately the coordinate system is different for the inversion of each sample. A right handed *xyz* Cartesian coordinate system is used. The origin of the coordinate system is on the Earth's surface directly below the centre of the transmitter loop. The x-axis is in the direction of flight of the aircraft at that sample location, the y-axis is in the direction of the left wing and the z-axis is directed vertically upwards (convention bottom right corner Figure 2).

System geometry

Pitch, roll and yaw are three angles that define the orientation of the transmitter loop moment vector (only pitch and roll are measured). The pitch and roll are the angles measured between the transmitter loop and the horizon, the pitch angle is defined as a measure of rotation about the x-axis, and the roll angle is the

rotation about the y-axis. Both pitch and roll are zero when the z-axis is vertical. The convention adopted by Spectrem Air is that aircraft nose up indicates a positive pitch angle, and aircraft left wing up indicates a positive roll angle. The order of operations for calculating the vector orientations is to apply the pitch, roll then yaw rotations respectively.

By taking tilt measurements on the ground Spectrem Air have established that the airplane tilt angle meters give correct angles for the Tx-loop, to within 0.01°. We assumed that radar altimeters can measure with accuracy of up to 1 m; therefore, when inverting SPECTREM data we have allowed the inversion to solve only for vertical and horizontal Tx–Rx separation and for receiver coil pitch.

The centre of the transmitter loop is located at (0, 0, TX_h). Roll of the transmitter loop (TX_r) is defined as anti-clockwise rotation, about an axis through (0, 0, TX_h) and parallel to the x-axis, so that a positive roll will bring the left wing up. Pitch of the transmitter loop (TX_p) is defined as anti-clockwise rotation, about an axis through (0, 0, TX_h) and parallel to the y-axis, so that positive pitch will bring the aircraft's nose down. Yaw of the transmitter loop (TX_y) is defined as anti-clockwise rotation, about an axis through (0, 0, TX_h) and parallel to the z-axis, so that a positive yaw would turn the aircraft left. However since the x-axis is defined to be in the direction of flight at each sample, the transmitter loop yaw is always zero by definition.

Note that transmitter loop pitch data supplied by Spectrem Air uses the convention where a positive transmitter pitch is nose up, and accordingly the supplied pitch is reversed in sign before being used in the inversion algorithm.

The position of the receiver coils relative to the transmitter loop is defined by the transmitter to receiver horizontal inline separation (D_x), the transmitter to receiver horizontal transverse separation (D_y), and the transmitter to receiver vertical separation (D_z), The receiver coils are thus located at (D_x, D_y, RX_h=TX_h+D_z). The receiver coils are always behind and below the aircraft (D_x<0, D_z<0). The receiver coils' roll (RX_r), pitch (RX_p) and yaw (RX_y) have the same rotational convention as for the transmitter loop except that they are rotations about the point (D_x, D_y, D_z). The receiver coils are always assumed to be located on the y-axis (D_y=0) and to have zero yaw (RX_y=0). Although this is not in reality the case, the position and orientation is not measured and there is not enough information available to solve for these since Y-component data is not available.

Layered earth

The layered earth model is independent at each inverted sample location. The layered earth consists of N_L horizontal layers stacked on top of each other in layer cake fashion. The k^{th} layer has constant thickness t_k and the bottom layer is a half-space that has infinite thickness ($t_{NL} = \infty$), extending to infinite depth. The electrical conductivity of the k^{th} layer is c_k and it is constant throughout the layer. The magnetic permeability of all layers is assumed to be equal to the magnetic permeability of free space μ_0. The dielectric permittivity of all layers is assumed to be equal to the permittivity of free space ε_0.

SPECTREM$_{2000}$ data

Because the transmitter of the SPECTREM system is continuously active during data acquisition, it is difficult to separate the transmitted primary field and secondary ground response from the measured total field. The separation process used by Spectrem Air is to record a high-altitude reference line, high enough to avoid the influence of ground response. Here, the assumption is that the reference data is effectively the

primary field convolved with the system response. Survey data subsequently collected are then processed by subtracting the high-altitude primary field.

Spectrem Air does not calibrate EM measurements in the sense that they make no laboratory measurements or calculations of the influence of the aircraft's self response, of precise Tx moment, or of the influence of analogue to digital conversion amplifier gain factors. No corrections for these (collectively referred to as system response) are applied.

Both X- and Z-components of the EM data are normalised by the corresponding estimated X- and Z-components of the primary field. The primary field is considered to be the magnetic field (normalised by the Tx dipole moment) due to a vertical dipole transmitter. The Tx–Rx separations provided by Spectrem Air are nominal horizontal and vertical separations derived from high-altitude flights. In their calculation of the primary field, Spectrem Air do not take into account the pitch and roll of the Tx loop, which they assume to be zero.

In the conventional process to separate the system response and primary field from the secondary field, the last (tenth) window (the coupling channel) of the EM decay is subtracted from each of the earlier windows, in an attempt to remove the remanent primary that is present in the EM decay. The underlying assumption is that at very late times, the secondary field (i.e., earth response) is practically zero, and what remains is only the coupling coefficient. This assumption is reasonable in resistive areas, although evidence of remanent primary field effects on SPECTREM data have been noted (Smiarowski et al., 2010) in conductive areas.

Over very conductive environments, as is the case for much of Australia, this assumption breaks down because of large-amplitude ground responses through all time channels. The later time windows (the latter part of the decay) can still contain significant contributions from the secondary field. Hence, subtraction of the coupling channel can remove meaningful parts of the secondary field. Since acquisition of the Musgrave Province data in early 2012, Spectrem Air have modified their conventional processing to overcome this problem (du Plooy, personal communication, September 2012).

The modifications aim to obtain a better approximation of the coupling coefficient before subtracting it from the EM windows. Over conductive areas, the coupling coefficient so determined is typically smaller than that obtained by the previous processing method. Thus, for the new processing approach, subtraction of the coupling coefficient from the preceding EM windows produces larger response amplitudes than previously. This alternative coupling coefficient is obtained by a numerical process in which a sum of exponentials is fitted to the raw EM decay, that is, by exponential fitting.

Data processed with exponential fit was not provided by Spectrem Air for the Musgrave Province survey, presumably because they deemed resistivities to be high enough for the last window subtraction assumption to hold.

SPECTREM data are recorded, stacked and binned into nine windowed data transients for both X- and Z-components. Typically, the airspeed during SPECTREM surveys is 220 km/h. A subsample is drawn from the data every 0.1 or 0.2 s, corresponding to readings at 6 to 12 m intervals along the flight line.

To avoid the problems associated with the conventional method of separating the measured total field into primary and secondary fields during processing, it is the total field that is inverted. Spectrem Air have supplied secondary field window data only in ppm. We reconstructed the total field window data by calculating the primary field and then adding it back to the supplied secondary field. The primary field was

calculated using dipole equations (12) and (13) derived by Wait (1982), using the high-altitude receiver position estimates, as follows:

$$\frac{B_x^P}{M} = \frac{3\mu rz}{4\pi R^5}$$

where B_x^P is the calculated X-component of the primary magnetic field (X-reference primary field), *M* is the transmitter dipole moment, *r* is the horizontal Tx–Rx separation, *z* is the vertical Tx–Rx separation, R=sqrt(r^2+z^2) and $\mu/4\pi=10^{-7}$.

B_z^P is the calculated Z-component of the primary magnetic field (Z-reference primary field), where

$$\frac{B_z^P}{M} = \frac{\mu}{4\pi}\left(\frac{2z^2 - r^2}{R^5}\right)$$

The reconstructed X- and Z-component total field data for all sample windows are $B_T = B_x^p + B_x^s$ and $B_T = B_z^p + B_z^s$, respectively, where the superscripts *P* and *S* constitute the primary and secondary field components. Since Spectrem Air sampled each decay with nine windows, the measured (observed) data d^{obs} vector, of length $\boldsymbol{N_D} = 2 \times N_W = 18$, used in the inversion process is:

$$\boldsymbol{d^{obs}} = [X_1 X_2 \ldots X_{Nw} Z_1 Z_1 \ldots Z_{Nw}]^T$$

where ^{T} represents the matrix and vector transpose operator.

Noise levels

Noise levels for each window and receiver component in Figure A1, were calculated as standard deviations of the Gaussian error distribution of an additive plus multiplicative noise model following methodology proposed by Green and Lane (2003). The noise model parameters were determined from the high-altitude flights. Each X- and Z-component has an associated noise level, represented by an element of each window, grouped in noise vector d^{err} composed of 18 parts.

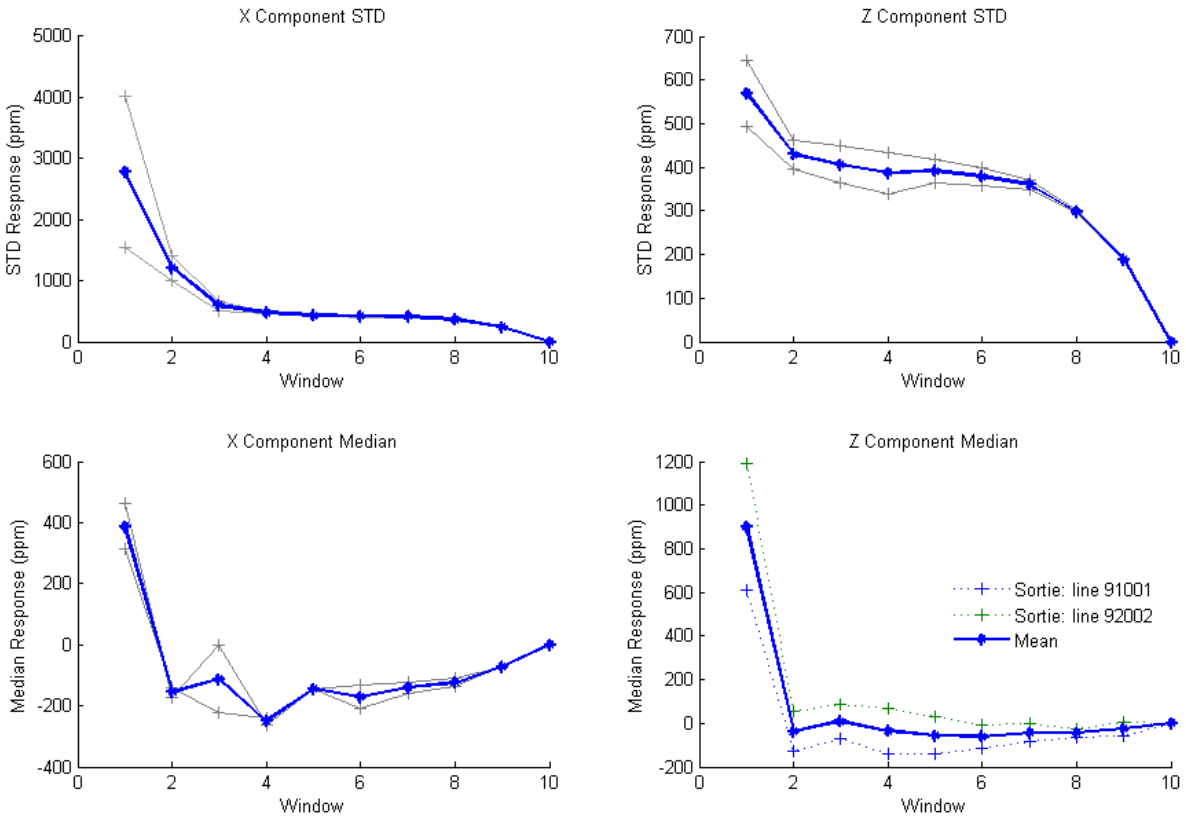

Figure A1. Noise levels for each window of both X and Z components estimated during high-altitude flight, assuming the signal is recorded in the absence of ground response.

Model parameterisation

The unknown model parameter vector (**m**) to be solved for in the inversion comprises earth model parameters and system geometry model parameters.

For the inversion of the SPECTREM dataset described here we used both a multi-layer smooth-model formulation(Constable et al., 1987) and a few-layer blocky-model formulation (Sattel, 1998). Therefore in the former we solve for the N_L conductivities of the layers, and the latter we also solve for thicknesses. The layer thicknesses are inputs into the algorithm and are kept fixed throughout. To maintain positivity of the layer conductivities we actually invert for the base ten logarithms of the conductivities of each layer.

We solve for N_G=3 system geometry parameters: the transmitter to receiver horizontal in-line separation (D_x), the transmitter to receiver vertical separation (D_z), and the pitch of the receiver coil assembly (RX_p).

The unknown model parameter vector of length $N_P=N_G + N_L$ to be solved for is the concatenated vector of log base ten layer conductivities $\mathbf{lc} = [\log c_1 \;\; \log c_2 \;\; \cdots \log c_{N_L}]^T$ and the geometry parameters $\mathbf{g} = [D_x \;\; D_z \;\; RX_p]^T$, such that,

$$\mathbf{m} = [\mathbf{lc} \mid \mathbf{g}] = [\log c_1 \;\; \log c_2 \;\; \cdots \log c_{N_L} \;\; D_x \;\; D_z \;\; RX_p]^T$$

Forward model

The forward model *f(m)* is the calculated theoretical total field data response of an AEM system flying above a layered earth, given a set of model parameters with known ***p*** (conductivity, elements of geometry) and unknown *m* (layer thicknesses, other components of system geometry, waveform, window positions, etc.). The unknown geometric parameters vary among recording systems; better control over them usually improves the ability of the inversion to fit the data.

The forward model is a non-linear multi-valued function, based on Wait's (1982) formulation, which developed frequency-domain field expressions for vertical and horizontal magnetic dipole sources above a horizontally layered-earth. The formulation assumes that contributions from dielectric permittivity and magnetic susceptibility are minimal compared to contributions from electrical conductivity, so they are set to be those of free space, $\varepsilon_k = \varepsilon_0$ and $\mu_k = \mu_0$, respectively. The formulation also does not account for the contribution of displacement currents.

The full-cycle transient (0.04 s) equivalent square current waveform Figure A2, to which SPECTREM data are processed, is linearly sampled at 38,400 Hz (1536 samples) and transformed to the frequency domain by fast Fourier transform (FFT). The secondary induced magnetic field (B-field) is calculated using five logarithmically equivalently spaced frequencies per decade (in the range 25–38,400 Hz), using equations A1 and A2 . The in-phase and quadrature components are then splined to obtain linearly spaced values at the same frequencies as the nodes of the FFT transformed current waveform. The B-field transient response for each sounding is the product of the convolved multiplication of the splined secondary B-field with the FFT transformed current waveform, followed by its inverse FFT.

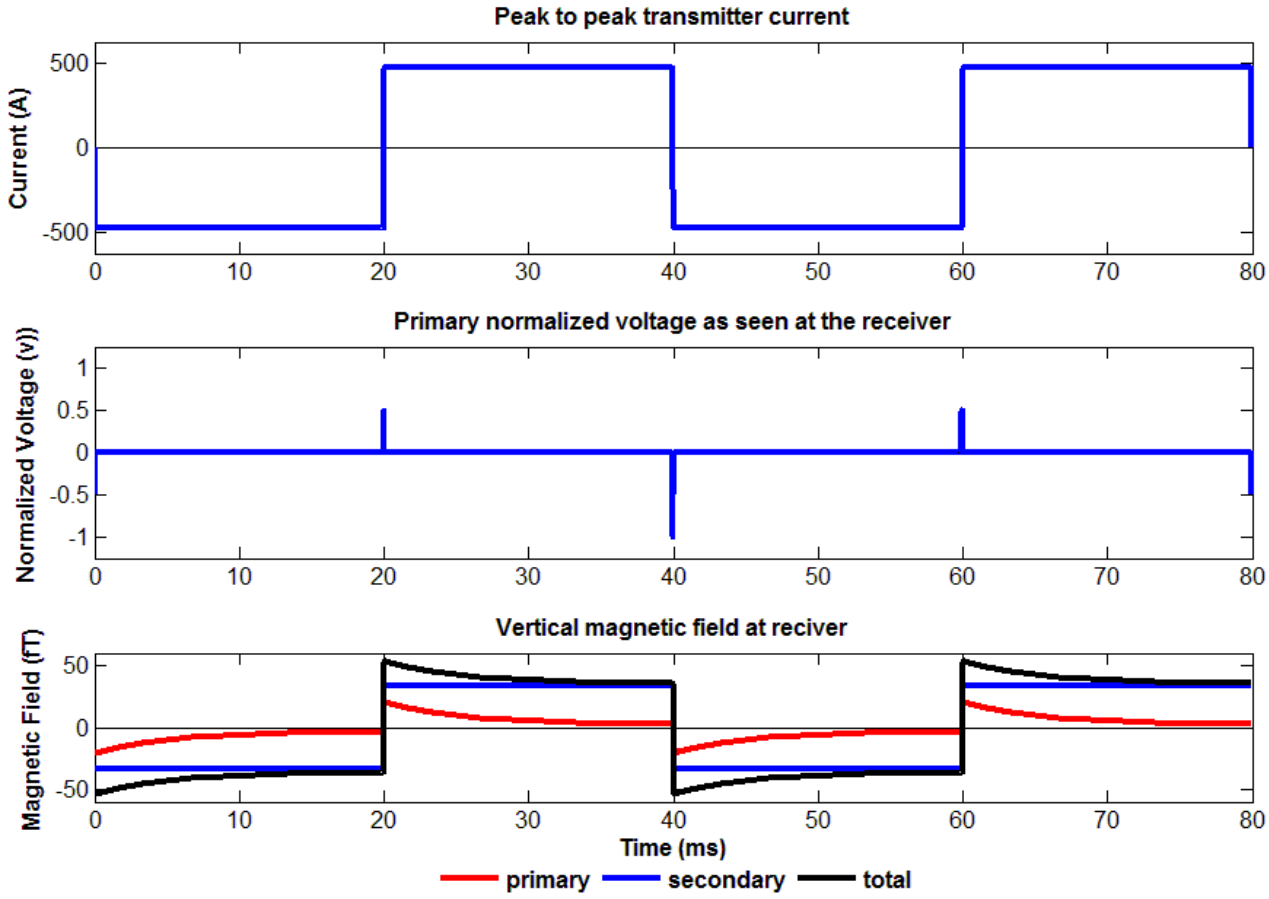

Figure A2. SPECTREM waveform showing a) transmitter current waveform, b) voltages at the receiver for the vertical Z component and c) vertical Z component of the magnetic B-field

The decay or transient response is then sampled and averaged with a boxcar filter into the nine windows specified in

Table 1. The computed primary and secondary fields are then added to produce the X- and Z-direction windowed total field. Finally, these windows are rotated and aligned with the axes of the X- and Z-component receiver coils in accordance with the receiver pitch model parameter.

Geoscience Australia's LEI inversion requires the partial derivatives of the Green's tensor of the primary field and reflection coefficients for individual layers. For computation of reflection coefficients, Brodie, (2010) used the propagation matrix method described by Farquharson and Oldenburg (1996) and Farquharson et al.(2003); to analytically calculate the primary field tensor partial derivatives.

Reference model

The inversion algorithm uses the concept of a reference model, with its corresponding uncertainties, to try to enforce inversion stability, mainly in places where prior information can be added to constrain parameters. The inversions herein have been carried out on a sample-by-sample basis; hence, the reference model provides only a soft or probabilistic constraint. If, from prior information, it is concluded that the likely distribution of the model parameter m_k is a Gaussian distribution with mean m_k^{ref} and standard deviation m_k^{unc}, then we would define the reference model vector as,

$$m^{ref} = \left[lc_1^{ref}\ lc_2^{ref}\ D_x^{ref}\ D_z^{ref}\ RX_p^{ref}\ \right]^T$$

and the reference model uncertainty vector as,

$$m^{unc} = \left[lc_1^{unc}\ lc_2^{unc}\ D_x^{unc}\ D_z^{unc}\ RX_p^{unc}\ \right]^T$$

The reference model mean values and uncertainties are inputs to the inversion algorithm and they may be different from sample to sample. The uncertainty values assigned to the reference model control the amount of constraint that the reference model places on the inversion results. A large uncertainty value for a particular parameter implies that the assigned reference model mean value is not well known and thus is allowed to vary a long way from the mean. On the other hand a low uncertainty implies the parameter is well known.

Objective function

The inversion scheme minimises a composite objective function of the form

$$\phi = \phi_d + \lambda(\alpha_c\phi_c + \alpha_g\phi_g + \alpha_{cv}\phi_v)$$

where ϕ_d is a data misfit term, ϕ_c is a layer conductivity reference model misfit term, ϕ_g is a system geometry reference model misfit term, and ϕ_v is a vertical roughness of conductivity term. The relative weighting of the data misfit and the collective model regularisation term ϕ_m is expressed by

$$\phi_m = (\alpha_c\phi_c + \alpha_g\phi_g + \alpha_{cv}\phi_v)$$

and is controlled by the value of regularisation factor λ. The three model regularisation factors (α_c, α_g and α_{cv}) control the relative weighting within the model regularisation term ϕ_m.

Data misfit parameter ϕ_d

Parameter ϕ_d is important; it provides an indication of how well the proposed layered-earth models represent the measured survey data at each sounding point. It is to some extent a measure of agreement between the observed data d^{obs} and the forward model produced by the model parameters described by *f(m),* which are normalised by the expected error and the number of data as defined by

$$\phi_d = \frac{1}{N_D}\sum_{k=1}^{N_D}\left(\frac{d_k^{obs} - f(m)}{d_k{}^{err}}\right)^2 = [d^{obs} - f(m)]^T W_d [d^{obs} - f(m)]$$

where W_d is the diagonal matrix $N_D \times N_D$

$$W_d = \frac{1}{N_d}\begin{bmatrix} \frac{1}{(d_1^{err})^2} & & \\ & \frac{1}{(d_2^{err})^2} & \cdots \\ & & \frac{1}{(d_D^{err})^2} \end{bmatrix}$$

Reference conductivity model misfit

The conductivity reference model misfit term ϕ_c is a measure of the misfit between the logarithmic conductivity base-ten model parameters lc and the corresponding layer reference model values lc^{ref}, normalised by the layer thicknesses and reference model uncertainty. It is defined as

$$\phi_c = \sum_{k=1}^{N_L}\frac{t_k}{T/N_L}\left(\frac{lc_k^{ref} - lc_k}{lc_k{}^{unc}}\right)^2 = \left[m^{ref} - m\right]^T W_c \left[m^{ref} - m\right]$$

where $T = \sum_{k=1}^{N_l} t_k$ and the $N_p \times N_p$ matrix :W_c:

$$W_c = \frac{N_L}{T}\begin{bmatrix} \frac{t_1}{(lc_1^{unc})^2} & & & & & & & \\ & \cdots & & & & & & \\ & & \frac{t_{NL-1}}{(lc_{NL-1}^{unc})^2} & & & & & \\ & & & \frac{t_{NL}}{(lc_{NL}^{unc})^2} & & & & \\ & & & & 0 & & & \\ & & & & & 0 & & \\ & & & & & & 0 & \end{bmatrix}$$

Because the bottom layer is infinitely thick, $t_{NL} = {[t_{NL-1}]^2}/{t_{NL-2}}$

System geometry reference model misfit

The system geometry reference model misfit term ϕ_g is a measure of the misfit between the data acquisition system geometry model parameters (g) and the corresponding system geometry reference model values (g^{ref}) are normalised by the number of unknown system geometry parameters (NG = 3) and their uncertainty. It is defined as

$$\phi_g = \frac{1}{N_G}\sum_{k=1}^{N_G}\left(\frac{g_k^{ref} - g_k}{g_k{}^{unc}}\right)^2 = \left[m^{ref} - m\right]^T W_g \left[m^{ref} - m\right]$$

where W_g is the diagonal matrix $N_p \times N_p$

$$W_d = \frac{1}{N_g}\begin{bmatrix} 0 & & & & & & & \\ & 0 & & & & & & \\ & & \cdots & & & & & \\ & & & 0 & & & & \\ & & & & 0 & & & \\ & & & & & \frac{1}{(D_x^{unc})^2} & & \\ & & & & & & \frac{1}{(D_y^{unc})^2} & \\ & & & & & & & \frac{1}{(RX_p^{unc})^2} \end{bmatrix}$$

Vertical roughness of conductivity

The vertical roughness of conductivity term ϕ_v is a measure of the roughness of the conductivity profile. It sums the squared second derivative of the logarithm of the vertical conductivity profile, approximated by finite difference over adjacent layer triplets, taking into account the distance between layer centres. The result is normalised by the number of triplets (N_{L-2}) and is defined as\

$$\phi_v = \frac{1}{N_{L-2}} \sum_{k=2}^{N_{l-1}} \left(\frac{(lc_{k-1} - lc_k)}{1/2(t_{k-1} t_k)} - \frac{(lc_k - lc_{k+1})}{1/2(t_{k+} t_{k+1})} \right)^2 = m^T L_v^T L_v m$$

where L_v is the matrix $N_{L-2} \times N_p$

$$\mathrm{L}_v = \frac{1}{N_L - 2} \begin{bmatrix} \frac{1}{\mathrm{t}_1 + \mathrm{t}_2}\left(\frac{-1}{\mathrm{t}_1 + \mathrm{t}_2} + \frac{1}{\mathrm{t}_2 + \mathrm{t}_3}\right) & \frac{1}{\mathrm{t}_2 + \mathrm{t}_3} & \cdots & & \\ \frac{1}{\mathrm{t}_2 + \mathrm{t}_3} & \left(\frac{-1}{\mathrm{t}_2 + \mathrm{t}_3} + \frac{1}{\mathrm{t}_3 + \mathrm{t}_4}\right) & \frac{1}{\mathrm{t}_3 + \mathrm{t}_4} & & \\ & & & 0 & \\ & & & & 0 \\ & & & & & 0 \end{bmatrix}$$

Once again we have the recursive algorithm, $t_{NL} = {}^{[t_{NL-1}]^2}/_{t_{NL-2}}$

Minimisation scheme

Linearisation

In order to minimise the objective function ϕ, a linearised gradient-based iterative minimisation scheme was used. By collecting the matrix notation misfit terms (equations A9, A11, A13 and A15) that constitute ϕ, we can write

$$\begin{aligned} \phi(m) = [d^{obs} - f(m)]^T W_d [d^{obs} - f(m)] \\ + \lambda \alpha_c [m^{ref} - m\ ]^T W_c [m^{ref} - m\ ] \\ + \lambda \alpha_g [m^{ref} - m\ ]^T W_g [m^{ref} - m\ ] \\ + \lambda \alpha_v m^T L_v^T L_v m \end{aligned}$$

The inversion begins by setting the initial estimate of the model parameters to the reference model, $m_0 = m^{ref}$. During the n^{th} iteration, the current estimate of the model parameters m_n is perturbed by the parameter change vector

$$\Delta m_n = m_{n+1} - m_n$$

The forward model at the new set of model parameters m_{n+1} is approximated by a Taylor series expansion about m_n, which, after excluding high-order terms, reduces to

$$f(m_{n+1} \approx [f(m_n) - J_n(m_{n+1} - m_n)]$$

where $J_n = \partial f(m)/\partial m$ is the Jacobian matrix whose i^{th}, j^{th} element is the partial derivative of the i^{th} datum with respect to the j^{th} model parameter evaluated at m_n in model space. Making use of equation (A19) and substituting $m = m_{n+1}$ allows equation (A17) to be rewritten as

$$\begin{aligned}\phi(m_{n+1}) = [d^{obs} - f(m_n) - \mathrm{J_n}(m_{n+1} - m_n)]^T W_d [d^{obs} - -f(m_n) \\ - \mathrm{J_n}(m_{n+1} - m_n)] \\ + \lambda\alpha_c \left[m^{ref} - m_{n+1}\right]^T W_c \left[m^{ref} - m_{n+1}\right] \\ + \lambda\alpha_g \left[m^{ref} - m_{n+1}\right]^T W_g \left[m^{ref} - m_{n+1}\right] \\ + \lambda\alpha_v {m_{n+1}}^T L_v^T L_v m_{n+1}\end{aligned}$$

Since the value of ϕ is minimised when $\partial f(m)/(\partial m_{n+1}) = 0$, we differentiate equation (A20) with respect to m_{n+1}, and set the result to zero, giving

$$\begin{aligned}0 = -2J_n^2 W_d [d^{obs} - f(m_n) - J_n(m_{n+1} - m_n)] \\ +\lambda\left[-2\alpha_c W_c [m^{ref} - m_{n+1}\right] \quad - 2\alpha_g W_g \left[m^{ref} - m_{n+1}\right] \\ + 2\alpha_v L_v^T L_v m_{n+1}\end{aligned}$$

Collecting terms in the unknown vector m_{n+1} on the left-hand side produces

$$\begin{aligned}\left[J_n^T W_d J_n + \lambda(\alpha_c W_c + \alpha_g W_g + \alpha_v L_v^T L_v)\right] m_{n+1} \\ = J_n^T W_d \left[d^{obs} - f(m_n) - J_n m_n\right] \\ + \lambda\left[\alpha_c W + \alpha_c W_c \quad\right] m^{ref}\end{aligned}$$

Because equation (A22) is in the familiar form of a system of linear equations ($Am_{n+1} = b$), we can solve for m_{n+1} using various methods of linear algebra. The Cholesky decomposition was used here.

Choice of λ value

An initial value of λ is chosen such that the data and model objective functions have approximately equal weight. This is automatically realised by computing the ratio of the data and model objective functions from the reference model perturbed by 1%, and computing the ratio of the data and model misfits as follows:

$$\lambda_{intial} = \frac{\phi_d(f(1.01\ m_0)}{\phi_m(1.01\ m_0)}$$

Then at each iteration the inversion employs a 1D line search where, to solve for m_{n+1} in equation (20), different values of λ are trialled until a value of λ_n is found such that

$$\phi_d\big(f(m_{n+1})\big) \approx \phi_d^{target} = 0.7|\phi_d\big(f(m_n)\big)$$

thus reducing to 0.7 of its previous value.

Convergence criterion

Iterations continue until the inversion terminates when one of the following conditions is met:

- ϕ_d reaches a user-defined minimum value,
- ϕ_d has been reduced by less than 1% in two consecutive iterations, or
- ϕ_d can no longer be reduced, or the number of iterations reaches a maximum of 100.

Appendix III: Thickness and corresponding depths for the 30 layer model

Table A3. 1 Thirty-layer fixed layer thickness model

Layer	Thickness (m)	Depth to base (m)
1	2.00	2.00
2	2.20	4.20
3	2.42	6.62
4	2.66	9.28
5	2.93	12.21
6	3.22	15.43
7	3.54	18.97
8	3.90	22.87
9	4.29	27.16
10	4.72	31.88
11	5.19	37.07
12	5.71	42.78
13	6.28	49.06
14	6.90	55.96
15	7.59	63.55
16	8.36	71.90
17	9.19	81.09
18	10.11	91.20
19	11.12	102.32
20	12.23	114.55
21	13.46	128.00
22	14.80	142.80
23	16.28	159.08
24	17.91	176.99
25	19.70	196.69
26	21.67	218.36
27	23.84	242.20
28	26.22	268.42
29	28.84	297.26
30	∞	∞

GOYDER INSTITUTE FOR WATER RESEARCH

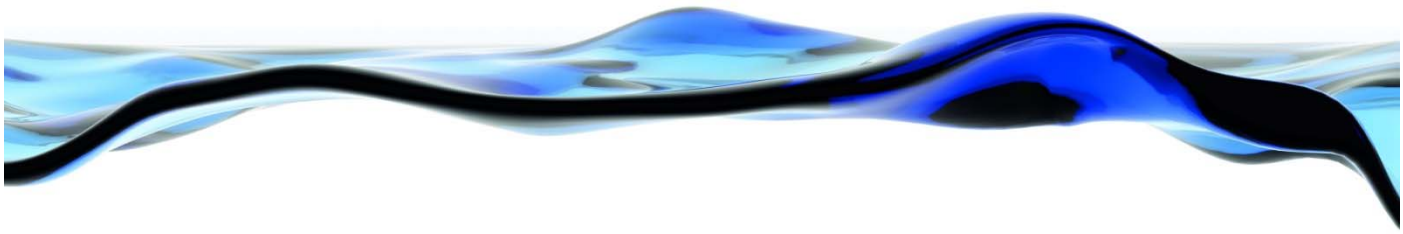

Government of South Australia
Department of Environment, Water and Natural Resources

CSIRO

THE UNIVERSITY of ADELAIDE

University of South Australia

Flinders UNIVERSITY ADELAIDE • AUSTRALIA

The Goyder Institute for Water Research is a partnership between the South Australian Government through the Department for Environment, Water and Natural Resources, CSIRO, Flinders University, the University of Adelaide and the University of South Australia.